Construction and Building Materials 409 (2023) 134070

Contents lists available at ScienceDirect

Construction and Building Materials

journal homepage: www.elsevier.com/locate/conbuildmat

Influence of activation temperature and prestress on behavior of Fe-SMA bonded joints

Lingzhen Li [a,b,*], Eleni Chatzi [b], Christoph Czaderski [a], Elyas Ghafoori [a,c]

[a] Empa, Swiss Federal Laboratories for Materials Science and Technology, Structural Engineering Research Laboratory, 8600, Dübendorf, Switzerland
[b] Institute of Structural Engineering (IBK), ETH Zürich, 8093, Zürich, Switzerland
[c] Institute for Steel Construction, Faculty of Civil Engineering and Geodetic Science, Leibniz University Hannover, 30167, Hannover, Germany

ARTICLE INFO

Keywords:
Memory steel (Fe-SMA)
Activation of prestress
Full-range behavior
Debonding
Local heating damage

ABSTRACT

The prestressed strengthening of structures via use of bonded iron-based shape memory alloys (Fe-SMAs) has proven promising, albeit with concerns regarding the temperature dependency of the adhesive properties. In this study, the effect of activation temperature and generated prestress are investigated experimentally. Six Fe-SMA-to-steel adhesively bonded joints, comprising different Fe-SMA strips (non-prestrained and prestrained) and activation strategies (full activation and partial activation), were prepared, activated via electrical resistance heating, and tested under quasi-static loading. It is found that the bond–slip behavior of a joint with activation can be modeled by that of an equivalent non-activated joint. The generated prestress influences the full-range behavior by raising the base tensile stress level of the Fe-SMA strip, with negligible effects on further aspects of the full-range behavior. With the increasing activation temperature, the fracture energy is initially increased and eventually reduced, while the bond capacity and effective bond length are retained almost constant.

1. Introduction

Existing infrastructures are constantly subjected to damaging and degradation effects, due to natural aging, environmental influences, and continually increasing and often repetitive loadings. The retrofitting and repair of such structures are essential means for ensuring their continued safety and functionality. In addition, given the high consumption of energy and raw materials in the construction sector [1,2], the retrofitting of existing structures reduces the need for replacement, thus serving the target of net-zero emissions.

Amongst available retrofitting techniques, prestressed strengthening enjoys a twofold benefit: (i) stiffness enhancement via addition of extra materials and (ii) introduction of prestress. Prestressed carbon fiber reinforced polymer (CFRP) strengthening, in particular, has attracted attention in the past two decades, owing to a high permissible prestress level and satisfactory E-modulus. Successful applications of prestressed CFRP strengthening focus on increasing the cracking and ultimate loads and reducing the crack width and deflection of reinforced concrete beams and slabs [3–5]; delaying or halting fatigue crack growth in steel structures [6–8]; and enhancing the buckling resistance of steel columns [9]. In these cases, the CFRP material is tensioned and then fixed onto/into the target structure; as soon as the tensile load is released, the tensile force in CFRP is balanced by the compression of the parent structure, and prestress is applied. During the afore-mentioned process, the tensioning (prestraining) and release (prestressing) are consecutively executed on-site, where a tensioning apparatus, such as a hydraulic jack, and an adequate space for operation are typically required.

Prestressing with shape memory alloys (SMAs), such as nickel-titanium based SMAs (NiTi-SMAs) and iron-based SMAs (Fe-SMAs), is a relatively new technique, in which the prestraining and prestressing processes are separated in time and space, by exploiting a special shape memory effect [10–12], as explained in the next paragraph. Applications of prestressed strengthening employing Fe-SMA strips and rebars or CFRP/NiTi-SMA composites deliver results that are similar to those with prestressed CFRP. This includes an increase in the cracking and ultimate loads and a reduction of crack width and deflection of concrete beams when employing Fe-SMA rebars/strips [13,14]. Additionally, Fe-SMA strips [15–17] and CFRP/NiTi-SMA composites [18–20] enhance the fatigue resistance of steel structures, significantly extending their fatigue lives, with some even halting the fatigue crack

* Corresponding author at: Empa, Swiss Federal Laboratories for Materials Science and Technology, Structural Engineering Research Laboratory, 8600, Dübendorf, Switzerland.
E-mail addresses: lingzhen.li@empa.ch (L. Li), chatzi@ibk.baug.ethz.ch (E. Chatzi), christoph.czaderski@empa.ch (C. Czaderski), ghafoori@stahl.uni-hannover.de (E. Ghafoori).

https://doi.org/10.1016/j.conbuildmat.2023.134070
Received 13 May 2023; Received in revised form 13 October 2023; Accepted 2 November 2023
Available online 8 November 2023

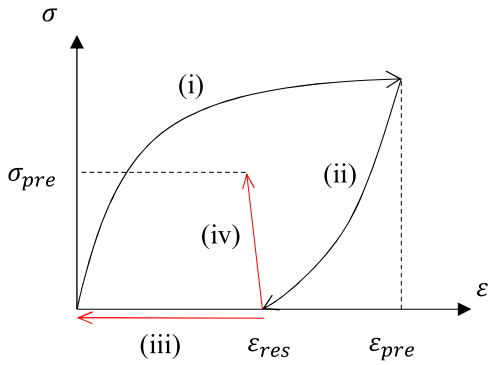

Fig. 1. Schematic prestressing process using Fe-SMA. Paths (i) prestraining, (ii) unloading, (iii) heating with free deformation (no prestress), and (iv) heating while restricting the deformation (with prestress). Arrows in red color reflect heating processes. (For interpretation of the references to color in this figure legend, the reader is referred to the web version of this article.)

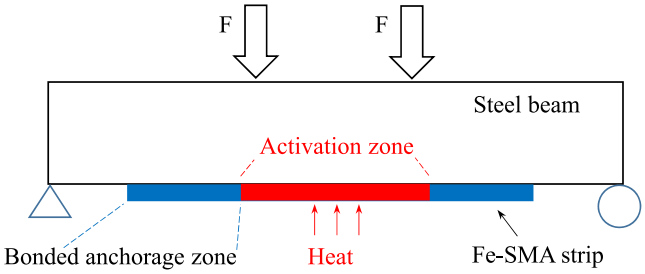

Fig. 2. Schematic view of a steel beam strengthened by means of bonded Fe-SMA with partial activation. (For interpretation of the references to color in this figure legend, the reader is referred to the web version of this article.)

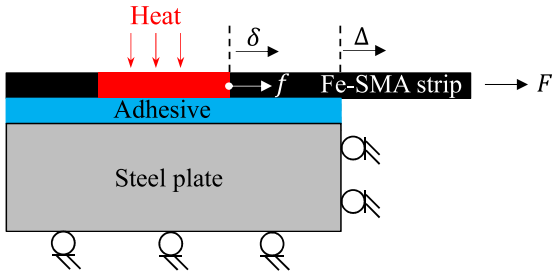

Fig. 3. Scheme of a lap-shear specimen with local activation. $F-\Delta$ refers to as the load–displacement behavior of the entire bonded joint, while $f-\delta$ refers to the (internal) force–displacement behavior of the activation zone. (For interpretation of the references to color in this figure legend, the reader is referred to the web version of this article.)

growth [15,17]. Compared with CFRP/NiTi-SMA composites strengthening, where CFRP provides extra stiffness and NiTi-SMA wires offer prestress, Fe-SMA combines both advantages.

Since the current study focuses on strengthening via use of Fe-SMA strips, an example on generating prestress is offered for the particular case of this material, as schematically illustrated in Fig. 1. The Fe-SMA strip is (i) tensioned to a prestrain level (ε_{pre}) and (ii) unloaded to a zero stress state, yielding a residual strain (ε_{res}); this process is referred to as prestraining, during which the elastic strain is revertible, while the residual strain (ε_{res}) remains. The residual strain contains a phase transformation strain, which is fully recoverable at a certain activation temperature, and a plastic strain, which is irrecoverable. For the sake of simplification, the residual strain is regarded as a phase transformation strain herein, while the plastic strain is ignored. Heating the prestrained Fe-SMA strip leads to two branches: (iii) in the case of a free deformation, the residual strain (ε_{res}) fully recovers, and the Fe-SMA strip returns to its original shape, demonstrating a "shape memory effect"; (iv) if the Fe-SMA strip is fixed onto/into a target structure, only a part of the residual strain recovers, and prestress (σ_{pre}) is generated in the Fe-SMA strip, while a balancing compression is generated in the parent structure. Different from traditional prestressing techniques, prestressing using Fe-SMA only requires on-site fixation to the target structures and heating, while the rest, such as the prestraining process, can be conducted offsite in a factory or laboratory. The apparatus required on-site can be minimized, facilitating the application of prestress. To heat the Fe-SMAs, typical techniques include electrical resistance heating [13], gas torch heating [21], and heating mats/pads [22].

The bonded strengthening of steel structures using Fe-SMA, which is schematically shown in Fig. 2, is deemed promising, as it offers further advantages in terms of (i) not damaging the parent structure and (ii) ensuring a gradual stress transfer between the substrate and strengthening material. In this system, guaranteeing a reliable bonding interface is fundamental. A considerable amount of knowledge has been built in the bonded anchorage zone, where the prestress is transferred to the steel substrate, via both experimentation on lap-shear joints [23,24] and corresponding modeling efforts [25]. During the activation process, the adhesive properties in the activation zone are affected by the elevated temperature, leading to a changed bond behavior, which necessitates further investigation.

This study investigates the influence of the activation temperature and generated prestress on the bond behavior between Fe-SMA strips and steel substrates, by means of Fe-SMA-to-steel adhesively bonded joints (schematically illustrated in Fig. 3). Six bonded joints were prepared, activated via electrical resistance heating, and tested under lap-shear loads. Among the six joints, four comprise non-prestrained Fe-SMA strips, aiming at the influence of activation temperature, while the remaining two consist of prestrained Fe-SMA strips, targeting the effects of both the activation temperature and generated prestress. The behavior is analyzed in terms of both the full-range and bond–slip behavior. Results are compared with equivalent bonded joints without activation, as derived from a previous study [24].

2. Experimental campaign

In this study, six lap-shear specimens with dimensions identical to those featured in a previous experimental study by the authors [24] were prepared, activated with electrical resistance heating, and tested under quasi-static tensile loads. Four specimens with non-prestrained Fe-SMA strips aim at investigating the influence of the activation temperature, while the remaining two specimens with prestrained Fe-SMA strips target the influence of both the activation temperature and the generated prestress.

2.1. Materials

2.1.1. Fe-SMA

Two types of Fe-SMA strips, with the composition of Fe-17Mn-5Si-10Cr-4Ni-1(V,C) (mass%) [26], are used in this study, namely the non-prestrained and prestrained Fe-SMA strips. The prestrained Fe-SMA strip was obtained via tensioning the non-prestrained Fe-SMA strip to a prestrain level (ε_{pre}) of 2%, followed by unloading to a zero-stress state, with a residual strain (ε_{res}) level of ca. 1.3%. The stress–strain behavior of the non-prestrained and prestrained Fe-SMAs is depicted in terms of dashed red and blue curves in Fig. 4, respectively, which were measured by means of dog-bone samples [24]. The solid black curve

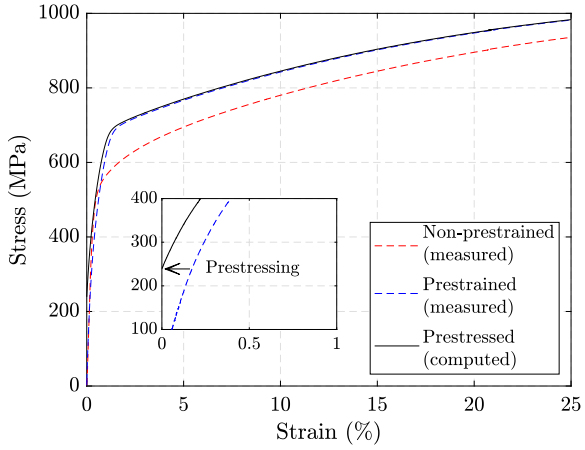

Fig. 4. The stress–strain behavior of Fe-SMAs. The dashed red and blue curves represent the measured non-prestrained and prestrained Fe-SMAs, while the solid black curve characterizes the computed behavior of the prestressed Fe-SMA with an activation temperature of 180 °C after the prestress loss. (For interpretation of the references to color in this figure legend, the reader is referred to the web version of this article.)

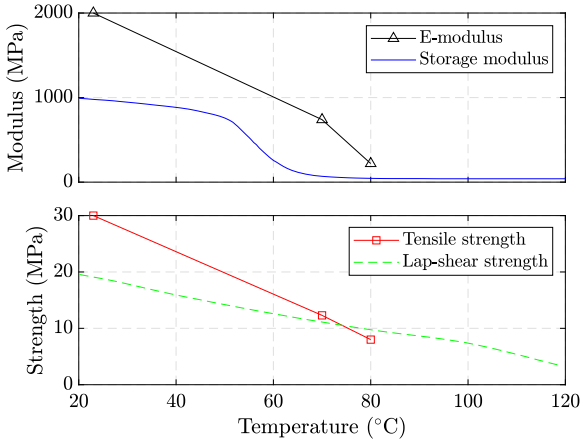

Fig. 5. Temperature dependent mechanical properties of SikaPower 1277. Data provided by the manufacturer [31,32], where the lap-shear strength was measured according to ISO 4587:2003 [34] using small lap-shear joints other than the one employed in the current study. (For interpretation of the references to color in this figure legend, the reader is referred to the web version of this article.)

reflects the stress–strain behavior of the prestrained Fe-SMA strip after activation with a target temperature of 180 °C, whose computation is introduced in the next paragraph.

A prestress analysis model [27], considering the prestress loss due to the shear deformation of the bond line and the compressive deformation of the steel substrate, was employed to compute the prestress level. According to previous studies, the stress–strain behavior of Fe-SMA, before and after prestressing, share an identical envelope [28–30]. Therefore, the stress–strain behavior of the prestressed Fe-SMA (solid black) was represented by the stress–strain of the prestrained Fe-SMA (dashed blue) truncated at the computed prestress level, as shown in the inset in Fig. 4. Two target temperatures of 180 and 260 °C were utilized in the activation tests, with the computed prestress levels being 239 MPa and 298 MPa, respectively.

2.1.2. Adhesive

The adhesive used in bonding, SikaPower 1277 (Sika AG, Switzerland), has an E-modulus of 1952 MPa, a tensile strength of 26.13 MPa, and an elongation at break of 4.37% at room temperature [24]. The glass transition temperature (T_g), around which the E-modulus drops drastically, is approximately 67 °C. The temperature has a huge impact on the mechanical properties of this adhesive, as visualized in Fig. 5. The E-modulus, tensile strength, and lap-shear strength at 80 °C reduce 89%, 73%, and 51%, respectively, compared with those at room temperature [31,32]. When further increasing the temperature, the storage modulus, which indicates the ability to store energy elastically [33], and lap-shear strength suffer additional reductions, while data on the evolution of the E-modulus and tensile strength are unavailable.

2.1.3. Steel

The steel plates of grade S355 comprise an E-modulus of 200 GPa, a tensile strength of 453 MPa, and an elongation at break of 23% [24].

2.2. Geometry and specimen preparation

Six lap-shear specimens were prepared, with the geometries shown in Fig. 6. The Fe-SMA strips have a length, width, and thickness of 600 mm, 50 mm, and 1.5 mm, respectively, while those of steel plates are 500 mm, 250 mm, and 10 mm, respectively. The bonded joint has a length of 300 mm and a thickness of 0.5 mm, while its width is identical to that of the Fe-SMA strip, i.e., 50 mm.

The bonding area of the Fe-SMA strips and steel plates were first cleaned with cotton-dipped acetone to remove the grease and dust, then sand-blasted to remove the oxidized layer and introduce some surface roughness, which was followed by another cleaning with cotton-dipped acetone. Pressed air was used to blow away the residual cotton fibers. The adhesive was then applied to bond the Fe-SMA strips and steel plates, and heavy weights were used to squeeze the excessive adhesive out, during which spacers with a thickness of 0.5 mm were used to control the thickness of the adhesive layer. The specimens were cured in a climate room with a constant temperature of 20 °C and a relative humidity of 50% for at least two weeks, prior to the activation tests.

2.3. Activation tests

After the curing of the bonded joints, the specimens, which can be divided into three groups according to their activation strategies, were activated by means of electrical resistance heating, as summarized in groups (i–iii) in Table 1 and Fig. 6.

Group (i): to investigate the effect of activation temperature on the bond behavior, two specimens with non-prestrained Fe-SMA strips were activated along the entire bond length, i.e., L_{act} = 300 mm. The two bonded joints in this group experienced debonding during the activation, which will be explained in Sections 4.1.3 and 4.3. No specimen with a prestrained Fe-SMA strip was activated along the entire bond length.

Groups (ii): to prevent the activation-induced debonding, two specimens with non-prestrained Fe-SMA strips were activated only in the middle 200 mm segment, with the remaining 50 mm length at each end set as the bonded anchorage zone, i.e., L_{act} = 200 mm and L_{anchor} = 50 mm.

Group (iii): to investigate the influences of both the activation temperature and the generated prestress, two specimens with prestrained Fe-SMA strips were activated in the middle 150 mm segment, with the remaining two ends (at 75 mm length) set as the bonded anchorage zone, i.e., L_{act} = 150 mm and L_{anchor} = 75 mm. Fig. 7 shows the activation of specimen PS-ACT260-1 in group (iii) as one example. After the activation process, specimens with prestrained Fe-SMA strips were expected to retain some level of prestress, while no prestress was expected in specimens with non-prestrained Fe-SMA strips.

It is worth noting that the testing configuration designed for activation tests, as shown in Figs. 6 and 7, does not fully reflect the loading

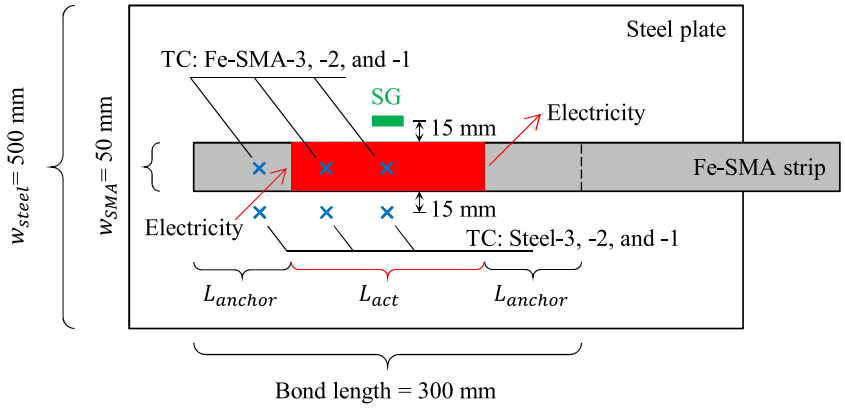

Fig. 6. Specimen geometries and activation strategies in groups (i–iii): (i) non-prestrained Fe-SMA with full activation, L_{act} = 300 mm and L_{anchor} = 0 mm; (ii) non-prestrained Fe-SMA with partial activation, L_{act} = 200 mm and L_{anchor} = 50 mm; and (iii) prestrained Fe-SMA with partial activation, L_{act} = 150 mm and L_{anchor} = 75 mm. The blue cross markers represent thermocouples (TC), while the green strip represents a strain gauge (SG), which applies only to groups (ii) and (iii). (For interpretation of the references to color in this figure legend, the reader is referred to the web version of this article.)

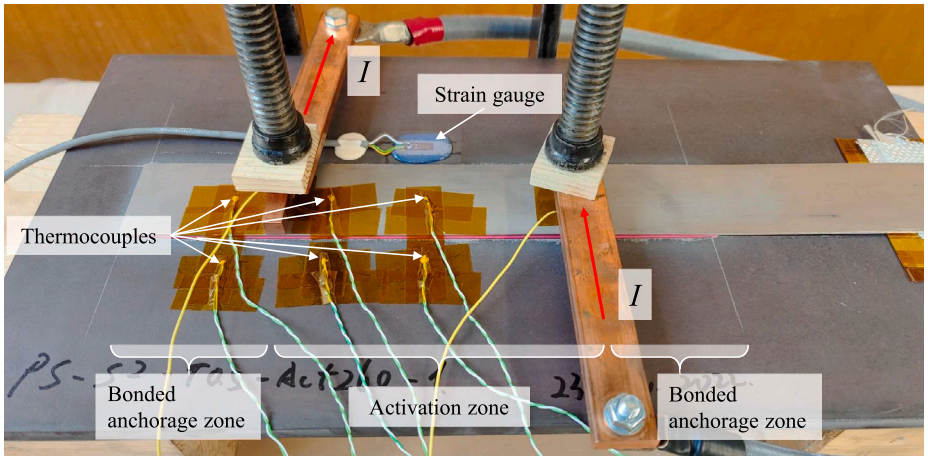

Fig. 7. Activation of specimen PS-ACT260-1. The two yellow cables connected to the electrical copper clamps aim at the voltage measurement over the activation zone. (For interpretation of the references to color in this figure legend, the reader is referred to the web version of this article.)

Table 1
Test matrix.

Groups	Specimen symbols	Types of Fe-SMA	L_{act} [a] (mm)	L_{anchor} [b] (mm)	T_{act} [c] (°C)	F_b [d] (kN)	L_{eff} [e] (mm)
(i)	NS-ACT180–1 NS-ACT260–1	Non-prestrained	300	0	180 260	N/A N/A	N/A N/A
(ii)	NS-ACT180–2 NS-ACT260–2	Non-prestrained	200	50	180 260	59.97 56.70	133 127
(iii)	PS-ACT180–1 PS-ACT260–1	Prestrained	150	75	180 260	63.29 62.41	122 118
(iv)	NS-ACT0-1[f] NS-ACT0-2[f]	Non-prestrained	N/A	N/A	N/A	59.09 58.93	121 125
(v)	PS-ACT0-1[f] PS-ACT0-1[f]	Prestrained	N/A	N/A	N/A	61.77 62.33	137 139

[a] L_{act} represents the activation length.
[b] L_{anchor} denotes the bonded anchorage length.
[c] T_{act} means the activation temperature.
[d] F_b is the bond capacity.
[e] L_{eff} represents the effective bond length.
[f] Specimens without activation are employed in this study for comparison purpose; they are denoted as NS-S2-T0.5-1, NS-S2-T0.5–2, PS-S2-T0.5–1, PS-S2-T0.5–2, respectively, in a previous experimental study [24].

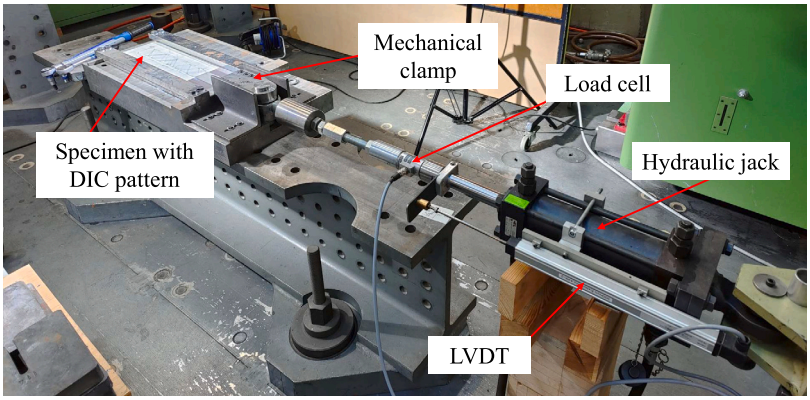

Fig. 8. Lap-shear test setup. (For interpretation of the references to color in this figure legend, the reader is referred to the web version of this article.)

pattern of prestressed strengthening for structures. An improved setup would involve heating the current activation zone and the bonded anchorage zone at the loaded end in Fig. 6, while the hydraulic jack holds the generated prestressing force, similar to activation tests of Fe-SMA rebars embedded in concrete blocks conducted by Schranz et al. [35]. However, the current study employed mostly metal components with good electrical conductivity, such as the Fe-SMA strip, steel plate, hydraulic jack, and supporting beam. If the activation tests are conducted on the lap-shear testing setup, while the hydraulic jack holds the generated prestressing force, the current employed for activation might accidentally damage laboratory equipment. Therefore, all activation tests were conducted according to Fig. 6, during which the specimens were supported by timber strips to ensure a proper electrical isolation. Even though the employed specimen configuration does not directly reflect the loading pattern of strengthening practice, a model proposed by the authoring team [27] is employed to analyze the prestressing behavior in Section 4.5.

During the electrical resistance heating, a direct current of ca. 500 A with an intensity of ca. 6.67 A/mm^2 was applied. Since the activation lengths of the Fe-SMA strips are different for each group, the measured voltages spanning over the activation lengths were ca. 3.5, 2.0, and 1.5 V in groups (i–iii), respectively. Three thermal couples (Fe-SMA-1, -2, and -3) were attached on the surface of Fe-SMA strips (two in the activation region and one in the anchorage zone) 25 mm away from the strips edge to monitor the temperature during the activation process, while three other thermal couples (Steel-1, -2, and -3) were attached on the corresponding locations and 15 mm away from the Fe-SMA strips edge. Once the target activation temperature, i.e., 180 or 260 °C, was reached in one of the thermal couples on the Fe-SMA strip, the electricity was stopped. In groups (ii) and (iii), a strain gauge was attached on the steel plate, 15 mm away from the edge of the Fe-SMA strip corresponding to the center of the activation zone, to examine whether the prestress was successfully generated. Note, a typical method of determining the applied prestress level is measuring the compressive strain on the substrate structure. However, due to the shear lag in the wide steel plate (500 mm in width), which is 10 times as wide as the Fe-SMA strip (50 mm in width), one strain gauge does not allow for a measurement of compressive strain state of the steel plate. Therefore, the single strain gauge only provides a sign of whether the prestress is generated.

Besides, four specimens in groups (iv and v) with the same geometries and materials but without activation from a previous study [24] are used for comparison purpose. In all five groups (i–v), lap-shear specimens comprise a constant bond length of 300 mm, while the activation lengths vary.

2.4. Lap-shear tests

After the activation, the black-speckled pattern on the white background was painted on specimens in groups (ii) and (iii), for the measurement of the full-field displacement and strain using a digital image correlation (DIC) technique during the lap-shear tests. Since the two specimens in group (i) experienced pronounced debonding during activation, they were not tested under mechanical loads. Therefore, no DIC pattern was prepared for them.

The steel plates of the four lap-shear specimens featuring DIC patterns were then fixed in a test setup, as shown in Fig. 8, while the Fe-SMA strips were tensioned toward the loading direction until a full debonding or rupture of the Fe-SMA strip. A displacement controlled loading regime was adopted, which allows for a gradual debonding (stable fracture) process. A hydraulic jack was employed to tension the Fe-SMA strips, while a load cell with a 150 kN capacity was used to measure the tensile force. A linear variable differential transformer (LVDT) was utilized to measure the displacement of the hydraulic jack, whose loading speed was controlled at 0.02 mm/s.

3. Post-processing

During lap-shear tests, the full-field displacement (U) and strain (ε) behaviors as well as the load–displacement behavior ($F-\Delta$) were measured, based on which the tensile stress of the Fe-SMA strip and the shear stress along the bond line can be inferred via the following steps. Similar procedures have been applied in studies of Fe-SMA bonded joints [23,24,36].

3.1. Tensile strain

During the DIC measurement, the full-field displacement and strain are presented in a 2D form, whose computation is cumbersome. Therefore, a two-point Gauss integral is utilized to approximate the measured 2D behavior by means of an equivalent 1D behavior, per Eq. (1).

$$\varepsilon_{mean} = \frac{\varepsilon_{-1/\sqrt{3}} + \varepsilon_{1/\sqrt{3}}}{2} \tag{1}$$

where ε_{mean} represents the average strain in the cross-section; $\varepsilon_{\pm 1/\sqrt{3}}$ are the strain values at the two Gauss points at $\pm w/2\sqrt{3}$ in the width direction, where w represents the width of the Fe-SMA strip.

3.2. Tensile stress

The tensile stress ($\sigma-x$) in the Fe-SMA strip is obtained by substituting the stress–strain behavior ($\sigma-\varepsilon$) into the measured strain behavior ($\varepsilon_{mean}-x$), with the following three cases differentiated:

1. Since no prestress is expected during the activation of a non-prestrained Fe-SMA strip, its mechanical behavior is assumed unaffected by the electrical resistance heating. Therefore, the stress–strain behavior, illustrated as red dashed curve in Fig. 4, of the non-prestrained Fe-SMA, is utilized to compute specimens with non-prestrained Fe-SMA strips in group (ii).

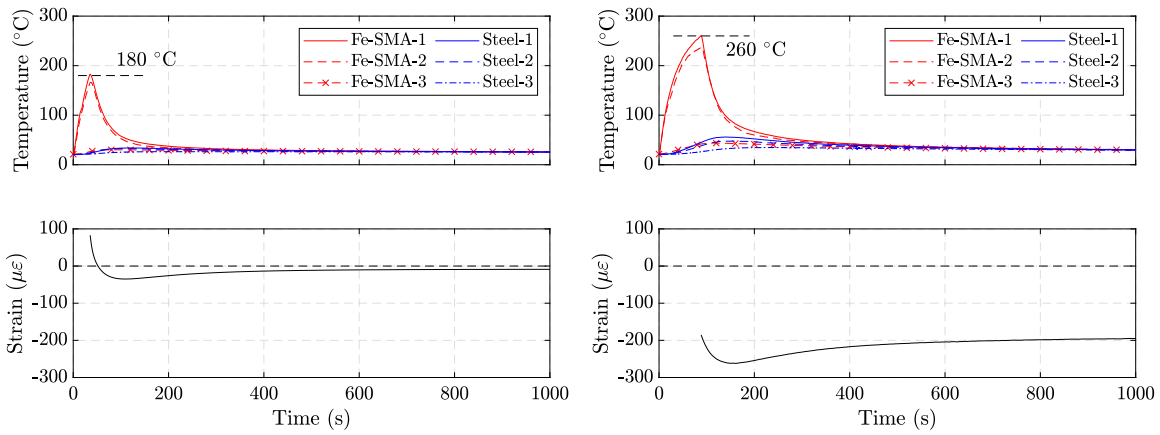

(a) Specimen NS-ACT180-2. (b) Specimen PS-ACT260-1.

Fig. 9. The measured temperature of the Fe-SMA strip (red) and steel plate (black) as well as the measured strain in the steel plate (black) changing with time. Please refer to Fig. 6 for locations of thermal couples and strain gauges. (For interpretation of the references to color in this figure legend, the reader is referred to the web version of this article.)

2. Specimens with prestrained Fe-SMA strips in group (iii). In the bonded anchorage zone, the temperature was only little influenced by the activation, with a maximum temperature of ca. 44 °C measured 25 mm away from the copper clamp. Therefore, the stress–strain behavior of the prestrained Fe-SMA, shown as the blue dashed curve in Fig. 4, is used to characterize the bonded anchorage zone.
3. In the meantime (group (iii)), prestress is generated in the activation zone via heating, therefore, the solid black curve in Fig. 4, representing a prestressed Fe-SMA strip, is assigned here.

3.3. Shear stress

Li et al. [36] proved, via 3D numerical simulations, that out-of-plane tensile stress is developed in the bond line of Fe-SMA-to-steel lap-shear joints. However, the contribution of the out-of-plane stress to the final fracture is negligible. Therefore, a simple equilibrium in the loading direction, per Eq. (2), is employed to compute the shear stress at the bottom of the Fe-SMA strip, which is identical to that in the bond line.

$$\tau = t \cdot \frac{\mathrm{d}\sigma}{\mathrm{d}x} \tag{2}$$

where σ and τ are the tensile and shear stresses, respectively; t and x denote the thickness of the Fe-SMA strip and the coordinate in the loading direction, respectively.

3.4. Bond–slip behavior

The bond–slip behavior ($\tau - s$), which is the shear stress (τ) as a function of the shear deformation (also known as the slip, s), is commonly used to characterize the behavior of adhesively bonded joints. The slip, which is the relative displacement between the Fe-SMA strip and steel plate in the loading direction, can be measured via the DIC technique. Synchronizing the computed shear stress and the measured slip at a specific location leads to the bond–slip behavior at this location. Repeating this process at different locations, the bond–slip behaviors along the entire bond line are obtained.

4. Results and discussions

4.1. Activation process

Figs. 9(a) and 9(b) illustrate the activation process of specimen NS-ACT180-2 in group (ii) and specimen PS-ACT260-1 in group (iii), respectively. The upper sub-figures demonstrate the temperature behavior of the Fe-SMA strip (red) and that of the steel plate (blue), while the lower sub-figures show the strain change on the steel plate next to the activation zone. Though comprising different Fe-SMA strips (non-prestrained and prestrained), specimens NS-ACT180-2 and PS-ACT180-1 share similar temperature behaviors during the activation. Likewise, specimens NS-ACT260-2 and PS-ACT260-1 possess alike temperature behaviors.

4.1.1. Activation of group (ii)

The temperature in the activation zone of the Fe-SMA strip (Fe-SMA-1 and -2) of specimens NS-ACT180-2, as illustrated in Fig. 9(a), went up rapidly toward the target temperature (180 °C) within 30 s, and soon dropped to ca. 70 °C, followed by a gradual reduction to the room temperature of ca. 20 °C. 25 mm away from the activation zone, the Fe-SMA strip (Fe-SMA-3) was heated to a maximum temperature of 30 °C, whose influence to the bond behavior is negligible. This means, the electrical resistance heating has a negligible influence on the bonded anchorage zone. Moreover, the temperature of the steel plate was raised to a maximum value of 35 °C ca. 2 min after the onset of activation, and then gradually decreased to the room temperature. During the electrical heating, no strain data was measured, due to the fact that the strain gauge cable was unplugged to prevent a damage to the strain measurement system caused by a penetration of the current from the activation system. Once the target temperature was reached, the electricity was cut off, and the strain measurement initiated. Shortly after the electrical heating was applied, a positive strain was measured, as visualized in Fig. 9(a), representing the thermal expansion of the Fe-SMA strip and steel plate. As the temperature was decreased, the strain in the steel plate was reduced, reflecting a reduced thermal expansion. Eventually, the strain on the steel plate kept a constant of -9 $\mu\varepsilon$, which could be attributed to (i) the redistributed thermal stress during heating and cooling and/or (ii) the generated prestress, due to the slight prestraining of Fe-SMA during the sand-blasting.

The strain behavior of NS-ACT260-2 is similar to that of NS-ACT180-2, with a measured strain of -5 $\mu\varepsilon$ at the end of activation. The observed temperature change during the activation is similar to that of specimens PS-ACT260-1, which is described in the next paragraph.

4.1.2. Activation of group (iii)

Fig. 9(b) illustrates the activation process of specimen PS-ACT260-1. Though the target temperature of 260 °C is ca. 44% higher than 180 °C, the time required to reach 260 °C was ca. 90 s, which is three times as that for reaching 180 °C. The reason is that a body

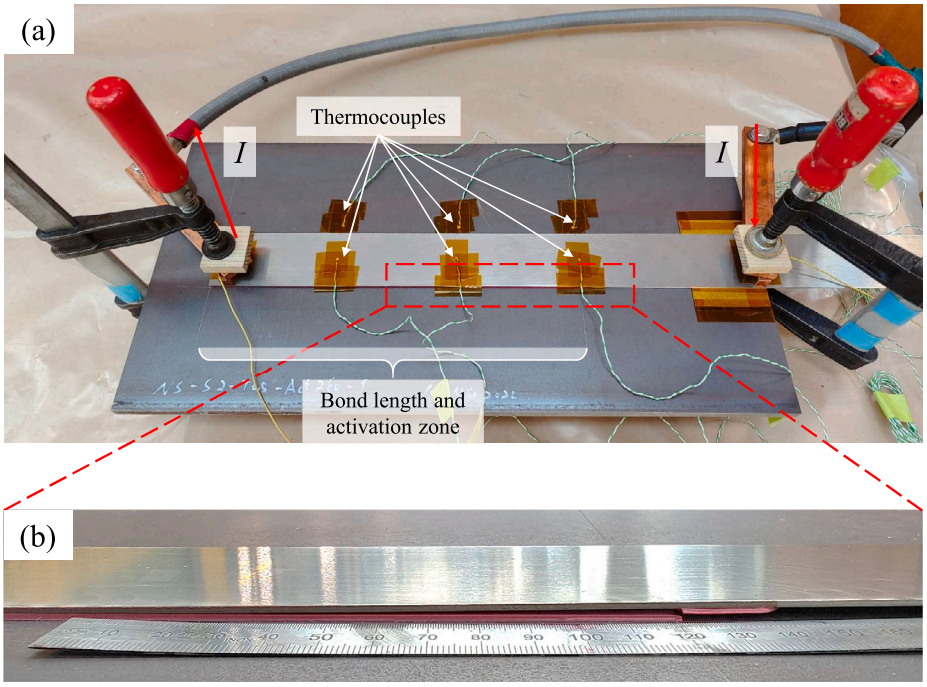

Fig. 10. Debonding during activation of joints with a full activation: (a) overview of specimen NS-ACT260-1, with an activation length of 300 mm (no strain measurement); (b) Side-view, a debonding of ca. 120 mm observed at the end of activation. (For interpretation of the references to color in this figure legend, the reader is referred to the web version of this article.)

with a higher temperature has a higher radiation to the environment, with more energy loss. Then, the temperature in the activation zone of the Fe-SMA dropped quickly to ca. 80 °C and gradually to the room temperature. The steel plate reached a maximum temperature of 56 °C ca. 140 s after the start of the activation. At the onset of the strain measurement, corresponding to a temperature of ca. 260 °C in the activation zone of the Fe-SMA strip, the steel was under compression with a measured strain of −185 $\mu\varepsilon$, which indicates the shape memory effect surpassing the thermal expansion. In the end, the strain gauge measured a compression of −191 $\mu\varepsilon$, suggesting a successfully applied prestress. In this specimen, a thermocouple (Fe-SMA-3) 25 mm away from the activation zone reported a maximum temperature of 44 °C. This means, the influence of the electrical resistance heating to the bonded anchorage zone can again be neglected.

The further specimen PS-ACT180-1 exhibits a similar temperature behavior to that of specimen NS-ACT180-2, while its strain behavior is similar to specimen PS-ACT260-1, with a stable compressive strain of −183 $\mu\varepsilon$ at the end of activation.

4.1.3. Activation of group (i)

In group (i), where the non-prestrained strips were activated over the entire bond length, as illustrated in Fig. 10(a), the temperature behaviors of specimens NS-ACT180-1 and NS-ACT260-1 are similar to those in Figs. 9(a) and 9(b), respectively. Since no bonded anchorage zone was set up, the thermocouple marked as Fe-SMA-3 also measured the temperature in the activation zone. During the electrical resistance heating (ascending of the temperature), the authors heard a clear cracking sound, suggesting debonding, which was then observed at the side of specimen, Fig. 10(b). Two major reasons exist for debonding during the activation, though no or negligible shape memory effect is expected in the non-prestrained Fe-SMA strips. A first cause may be attributed reduced bond capacity at an elevated temperature, while a second likely cause pertains to the generated thermal stress. A quantitative explanation is provided in Appendix.

4.2. Failure modes

Since specimens in group (i) experienced debonding during the activation, as demonstrated in Fig. 10(b), no lap-shear test was conducted in this group, leading to no discussion on their failure mode.

Fig. 11 presents the exposed fracture surfaces of the adhesive bonds after the lap-shear tests in group (ii). The specimen with an activation temperature of 180 °C (NS-ACT180-2) failed under a major cohesion and a minor adhesion mode, as shown in Fig. 11(a). The cohesion failure, which means the fracture occurring in the body of the adhesive layer, is a preferred failure mode, with which the design of bonded joints can be guaranteed by selecting a proper adhesive. On the other hand, the adhesion failure, which refers to the fracture at the adhesive-adherent interface, is less preferred, especially in the long-term performance; a larger amount of adhesion failure in the short-term is accompanied by a higher reduction of the bond capacity in the long-term, due to the penetration of moisture and salt [37]. Compared with the failure mode of the specimens without activation (group (iv)), which experienced mostly cohesion failure [24], the activation with heating and cooling introduced adhesion failure to some extent. This is similar to the failure mode of CFRP bond, where the elevated temperature changes the debonding mode from cohesion to adhesion [38,39]. At the junctions of the activation zone and bonded anchorage zone, where the copper clamps were pressed to improve the electrical conductivity, the color of the adhesive shifted from an originally pink to a slightly yellow shade. Further analysis of the local bond–slip behavior in coming sections suggests that the yellow color is an indication of changed bonding properties.

The other specimen in group (ii), corresponding to a higher activation temperature of 260 °C (NS-ACT260-2), even manifested local heating damage, which was visually inspected by the authors at the side of the specimen prior to the lap-shear test. The fracture surface of the adhesive layer, as demonstrated in Fig. 11(b), further confirms the local heating damage. In the activation zone, a major cohesion failure and a minor adhesion failure were again observed. In the meantime, the color of the adhesive was turned from an originally pink to a noticeably yellow shade.

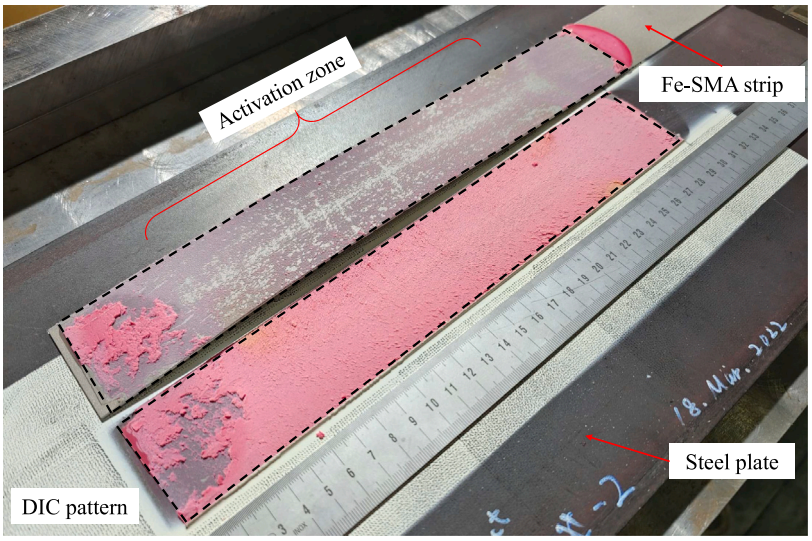

(a) $T_{act} = 180°C$, with specimen NS-ACT180-2 as an example.

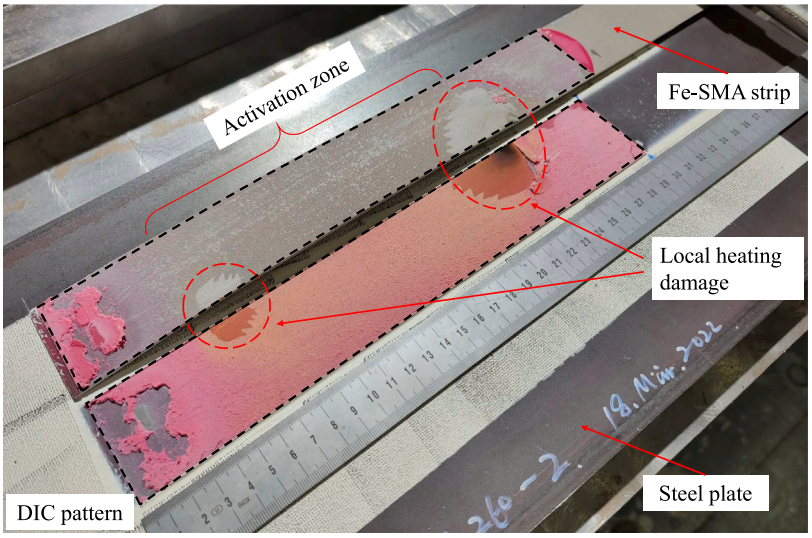

(b) $T_{act} = 260°C$, with specimen NS-ACT260-1 as an example.

Fig. 11. Failure modes with activation temperatures (T_{act}) of 180 and 260 °C. (For interpretation of the references to color in this figure legend, the reader is referred to the web version of this article.)

The failure modes of specimens in group (iii), under the effect of prestress, present highly alike failure modes compared with those in group (ii), which experienced no prestress. The elevated temperature in the activation zone introduced some adhesion failure, where the original pink color of the adhesive was turned yellow to some extent. At one of the locations attached with the copper clamp, the adhesive bond was damaged by the local excessive heating, as shown in Fig. 19. It can be concluded, based on these four specimens, that the activation temperature clearly introduces some adhesion failure, which is, however, not further affected by the generated prestress. The reason is that the prestressing force, which is majorly held by the bonded anchorage zone, can be regarded as an internal tensile load. Therefore, prestress should deliver a failure mode identical to those bonded joints without prestress.

4.3. Debonding behavior of group (i), with non-prestrained Fe-SMA and full activation

In group (i), where non-prestrained Fe-SMA strips were activated along the entire bond length, debonding occurred during the electrical resistance heating, as demonstrated in Fig. 10. A simplified 1D thermal analysis is conducted in this study, with the model setup and analysis detailed in Appendix. This analysis quantitatively explains that the thermal stress is the source of the debonding during activation.

The debonding during the activation suggests that an activation along the entire bond length leads to failure of the strengthening system, even with non-prestrained Fe-SMA, where no prestressing effect is expected. The survival of specimens in groups (ii) and (iii) during the activation tests highlights that the prevention of debonding during the activation necessitates bonded anchorage zones at the two ends of bonded strengthening. This is in line with the concept of partial activation proposed by Wang et al. [16].

4.4. Debonding behavior of group (ii), with non-prestrained Fe-SMA and partial activation

Specimens in groups (ii) and (iii) survived in the activation tests, due to the presence of the bonded anchorage zones, which resisted the thermal load during the ascending temperature and the prestressing load at the end of activation. After activation, lap-shear tests were conducted. The full-range bebavior, which refers to as the full-field

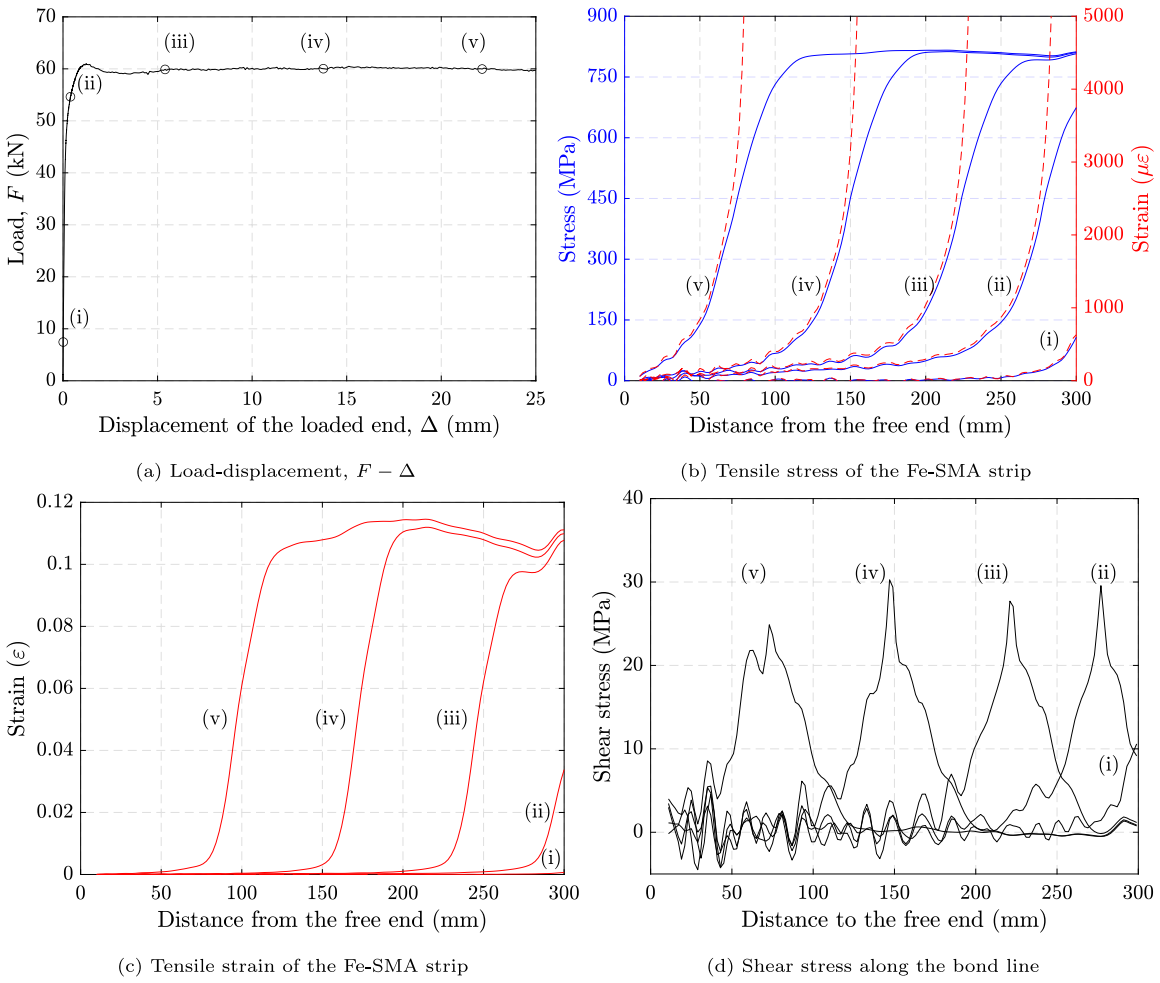

(a) Load-displacement, $F - \Delta$

(b) Tensile stress of the Fe-SMA strip

(c) Tensile strain of the Fe-SMA strip

(d) Shear stress along the bond line

Fig. 12. The full-range behavior of NS-ACT180-2, with a non-prestrained Fe-SMA strip and an activation temperature of 180 °C. Please refer to Fig. 3 for the definition of $F - \Delta$. (For interpretation of the references to color in this figure legend, the reader is referred to the web version of this article.)

behavior at different loading stages, is acquired via post-processing, as introduced in Section 3.

4.4.1. Specimen NS-ACT180-2

Fig. 12 depicts the full-range behavior of specimen NS-ACT180-2, with a non-prestrained Fe-SMA strip and an activation temperature of 180 °C. Despite the induced minor adhesion failure, the specimen with activation behaves almost identically to those without activation, NS-ACT0-1 and NS-ACT0-2 in group (iv) [24]. Its full-range behavior contains three stages: (i) the elastic stage, where most of materials behave elastically; (ii) the damage accumulation stage, where damage accumulates at the loaded end of the bonded joint; and (iii–v) the debonding propagation stage, where the tensile stress, tensile strain, and the shear stress profiles do not change shape, but propagate toward the free end, during which the tensile load is kept almost constant (corresponding to the bond capacity).

4.4.2. Specimen NS-ACT260-2

Fig. 13 shows the full-range behavior of NS-ACT260-2, with a non-prestrained Fe-SMA strip and an activation temperature of 260 °C. Its full-range behavior can still be characterized as three stages, but with some difference compared against the behavior without activation. Stages (i) and (ii) refer to the elastic and damage accumulation stages, respectively, similarly to the previous specimen. In stage (iii–v), the debonding propagation stage, the tensile strain, tensile stress, and shear stress profiles propagate to the free end. However, the shear stress peak disappears at x = 200–250 mm, which can be attributed to the local heating damage, as shown in the fracture surface depicted in Fig. 11(b). Correspondingly, the tensile stress and strain profiles at these locations are influenced.

Fig. 14 illustrates the local bond–slip behavior along the fracture surface. In each inset, the red curve represents the average bond–slip behavior of the bonded joint, while the black curves reflect the local bond–slip behavior, in this way reporting on the behavior across the entire width. At the center of the activation zone (x = 150 mm) and outside the activation zone (x = 280 mm), the local and average bond–slip curves are almost identical. In locations exhibiting a minor (x = 70 mm) and major local heating damage (x = 230 mm), the local bond–slip curves shrink in comparison with the average behavior. The shrinkage of the bond–slip behavior is a result of the excessive heating at the electrical copper clamp, as explained earlier. Such a local heating damage can be prevented via adoption of alternate activation strategies, such as the flame heating.

4.4.3. Comparison with non-activated specimens

Fig. 15 provides a comparison amongst the specimens comprising non-prestrained Fe-SMA strips, with and without partial activation. Despite slight deviations, the global load–displacement behaviors and local bond–slip curves of these joints are similar. This suggests that, regardless of the local heating damage, the behavior of bonded joints without activation can be adopted in joints with partial activation.

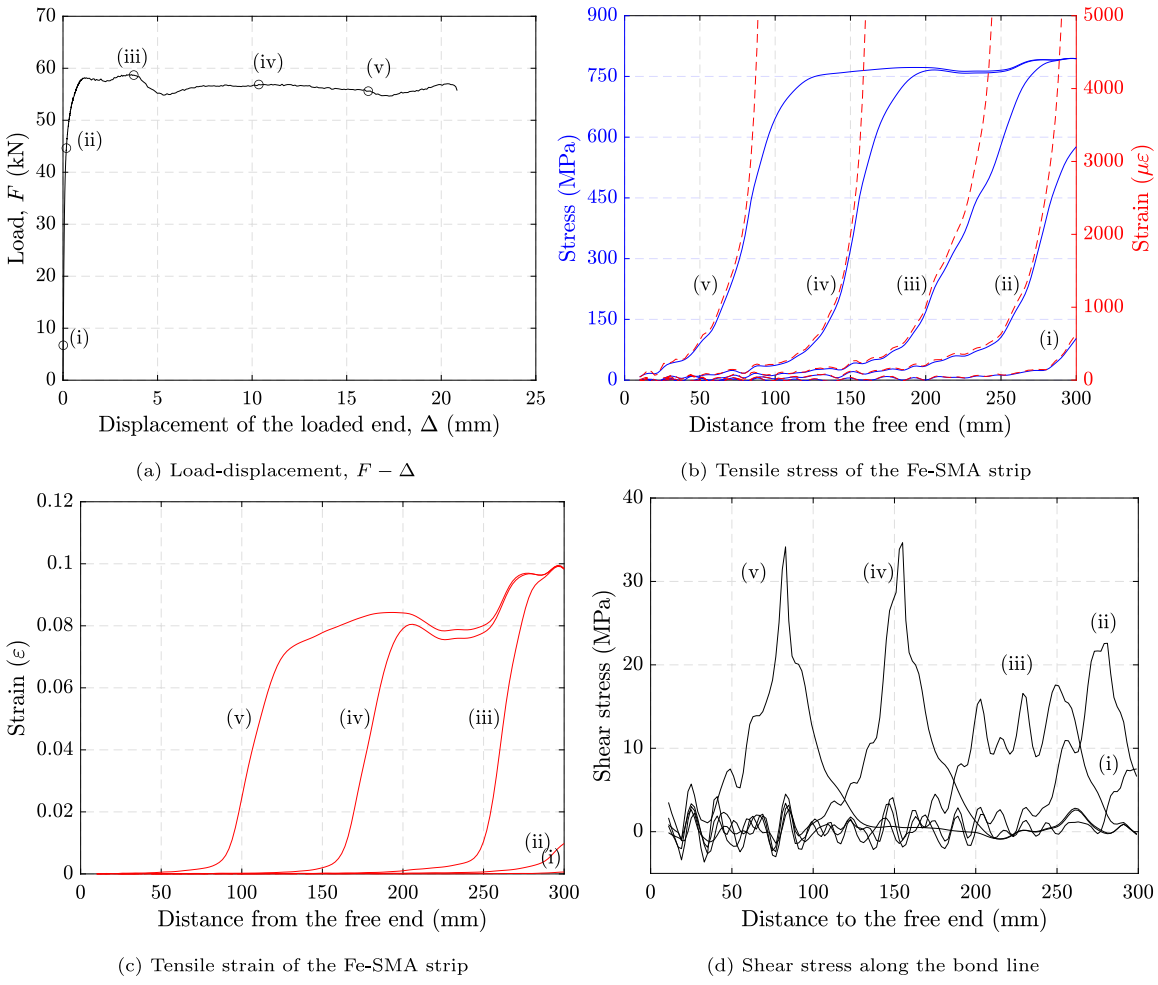

(a) Load-displacement, $F - \Delta$

(b) Tensile stress of the Fe-SMA strip

(c) Tensile strain of the Fe-SMA strip

(d) Shear stress along the bond line

Fig. 13. The full-range behavior of NS-ACT260-2, with a non-prestrained Fe-SMA strip and an activation temperature of 260 °C. Please refer to Fig. 3 for the definition of $F - \Delta$. (For interpretation of the references to color in this figure legend, the reader is referred to the web version of this article.)

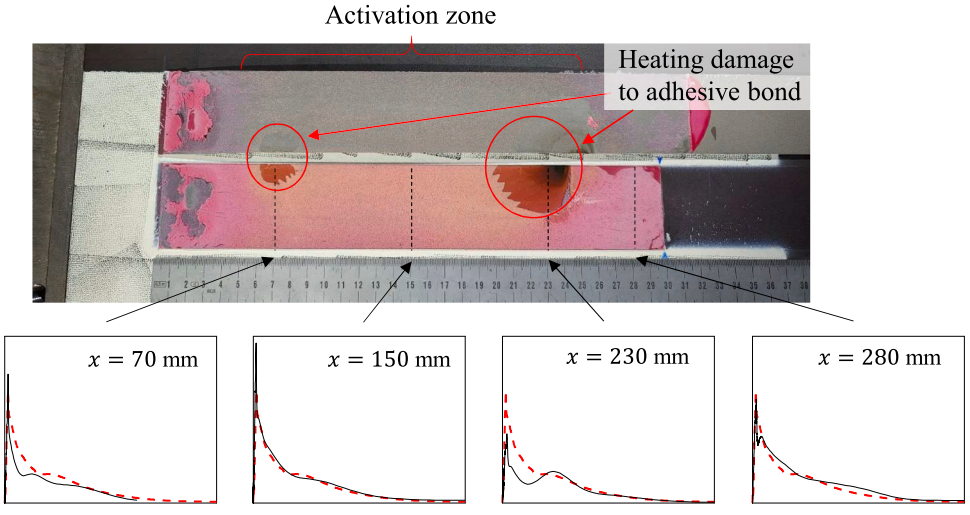

Fig. 14. The fracture surface of specimen NS-ACT260-2 and the measured bond–slip behavior. The dashed red curves are the average bond–slip behavior of the entire bond line, while the solid black curves are the local bond–slip behaviors. (For interpretation of the references to color in this figure legend, the reader is referred to the web version of this article.)

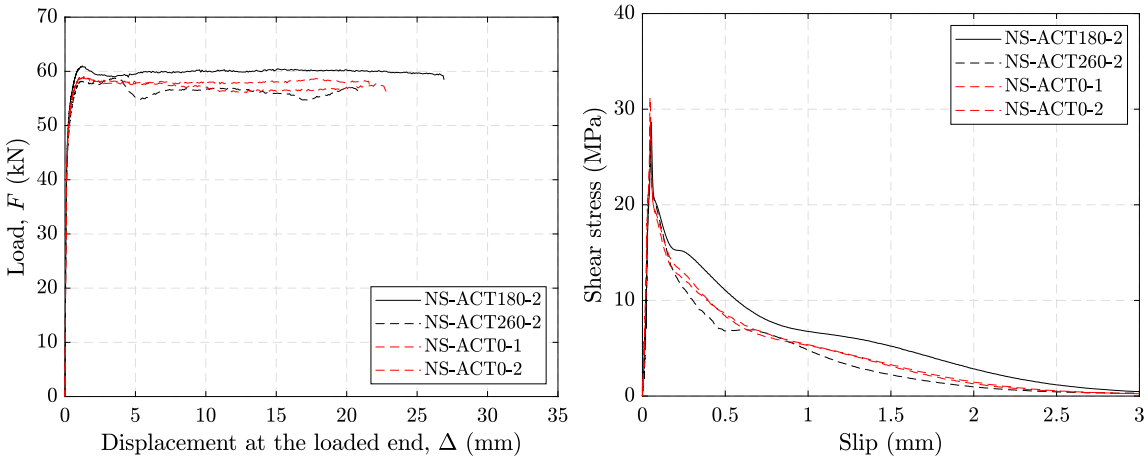

(a) Load-displacement, $F - \Delta$ (b) Bond-slip behavior

Fig. 15. Comparison among joints with activation (black) and without activation (red). Tensile forces are measured via a load cell. Please refer to Fig. 3 for the definition of $F - \Delta$. (For interpretation of the references to color in this figure legend, the reader is referred to the web version of this article.)

4.5. Debonding behavior of group (iii), with prestrained Fe-SMA and partial activation

In this group, the activation zone is designed with a length of L_{act} = 150 mm, which allows for development of an entire shear stress profile. Accordingly, the bonded anchorage zones comprise a length of L_{anchor} = 75 mm, which guarantees that the generated prestress does not incur debonding at this zone. Since the strain gauge attached on the steel plate does not allow for an accurate estimation of the prestress level, a model is used to compute the stress and strain state of specimens in this group. Given the explanation in Appendix that the adhesive layer during the activation has a negligible shear stiffness, it is assumed in this model that the adhesive is fully softened (zero shear stiffness) during the activation, and the generated prestress is retained by the bonded anchorage zones. As explained in Section 4.1, the activation temperature bears limited influence on the bonded anchorage zone. Therefore, the simplified bond–slip behavior at room temperature of the joints in group (v) [25], illustrated as dashed pink curve in Fig. 16, is employed to characterize the behavior in the bonded anchorage zone. The recovery stresses, which are the prestress measured by fixing the two ends of the prestrained Fe-SMA strips, corresponding to an activation to 180 and 260 °C are ca. 320 and 400 MPa, respectively [15,40–42]. Considering the prestress loss due to the limited shear stiffness at the bonded anchorage zone and the compression of the steel plate, the prestresses of specimens PS-ACT180-1 and PS-ACT260-1 are found to be 239 MPa and 298 MPa, respectively, as discussed in Section 2.1.1. Interested readers are referred to Ref. [27] for mathematics underpinning.

Fig. 16 depicts the stress and strain states of specimen PS-ACT180-1, after activation. The two bonded anchorage zones are loaded by the internal prestressing force. Since the bonded anchorage zone is shorter than the effective bond length of ca. 138 mm, the two ends (x = 0 mm and x = 300 mm) are slightly loaded with a non-zero shear stress. But, the adhesive in the bonded anchorage zones remains in the elastic region (ascending branch of the pink bond–slip curve). In the activation zone, the tensile stress plateau reflects the generated prestress from activation including the prestress loss; the prestress loss is visualized as the negative strain in the activation zone. Due to the assumption that the adhesive in the activation zone is fully softened and the bonded anchorage zone is not affected during the activation, the shear stress is zero at the activation zone, and a sharp shear peak occurs at the junction of the two zones. In reality, the peaks of the shear stress and tensile strain would be more gradual, due to the existence of the temperature gradient at the junctions and the stress redistribution during heating and cooling. After activation, the adhesive in the activation zone re-cures, as it resists shear load, which is explained in the next section.

4.5.1. Specimen PS-ACT180-1

The activation zone (x = 75–225 mm) is analyzed in this section, since both the elevated temperature and generated prestress are applied, forming the focus of the current study. The bonded anchorage zone (x = 0–75 mm and x = 225–300 mm) is always subjected to mechanical loads, with a negligible thermal effect, and its behavior is already known [23–25]. Therefore, the analysis of the bonded anchorage zone during the lap-shear test is excluded.

Fig. 17 shows the behavior at the activation zone of specimen PS-ACT180-1 during the lap-shear test. A significant difference, compared against the joints without activation (PS-ACT0-1 and PS-ACT0-2 in group (v) [24]), is the base tensile stress level of 239 MPa, which reflects the prestress generated during the activation test. Correspondingly, prior to the lap-shear test, the Fe-SMA in the activation zone already hold a tensile force of 17.97 kN. The full-range behavior in this zone can be categorized into three stages, similar to previous specimens. Stage (i) still refers to as the elastic stage; however, only the adhesive layer retains elasticity, due to the low shear stress level. The prestress level of 239 MPa exceeds the limit of proportionality, which is ca. 120 MPa [24]. In stage (ii), the damage accumulation stage, the stress and strain levels increase, and the damage accumulates at the loaded end, as the shear stress reduces after reaching a peak. In stage (iii–v), the debonding propagation stage, the tensile stress, tensile strain, and shear stress profiles do not change shapes but propagate to the further bonded anchorage zone (x = 75 mm). No apparent local heating damage is evident in the full-range behavior.

4.5.2. Specimen PS-ACT260-1

Fig. 18 demonstrates the full-range behavior at the activation zone of specimen PS-ACT260-1. Similar to the previous specimen PS-ACT180-1, the full-range behavior can be divided into three stages: (i) the elastic stage, (ii) the damage accumulation stage, and (iii–v) the debonding propagation stage. A major difference is the base tensile stress level has a higher value of 298 MPa.

Fig. 19 shows the fracture surface of the bonded joint of specimen PS-ACT260-1 and the computed local (black) and average (red) bond–slip behaviors in the activation zone. At location x = 104 mm, where a local heating damage occurred, the local bond–slip curve shrinks compared with the average curve. Other locations without the local heating damage, the local and average behaviors are almost identical.

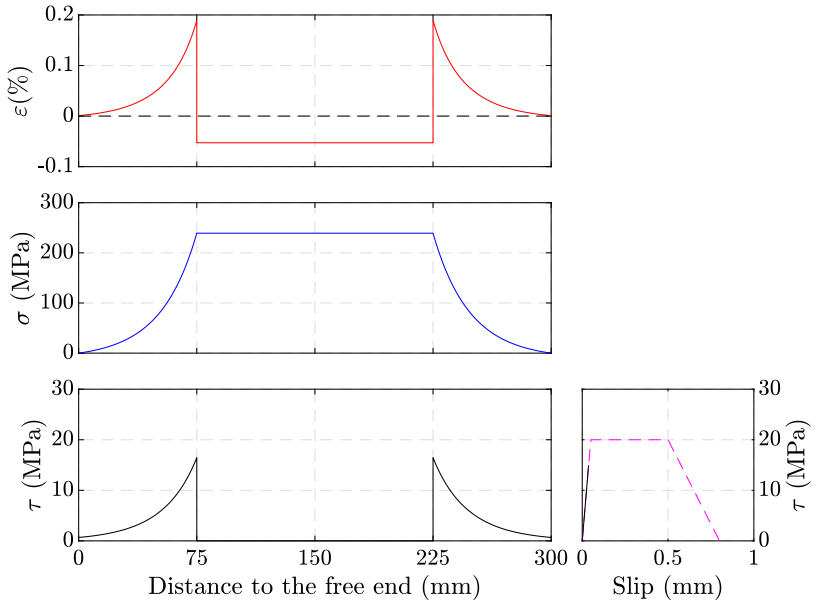

Fig. 16. The calculated stress and strain states of a bonded joint (PS-ACT180-1) after activation. The activation zone is located at $x = 75$–225 mm, while the two further regions reflect the bonded anchorage zones. The pink trapezoidal bond–slip curve [25] represents the bond behavior at the bonded anchorage zone, while the shear stress resisting the prestress is illustrated via a black curve. (For interpretation of the references to color in this figure legend, the reader is referred to the web version of this article.)

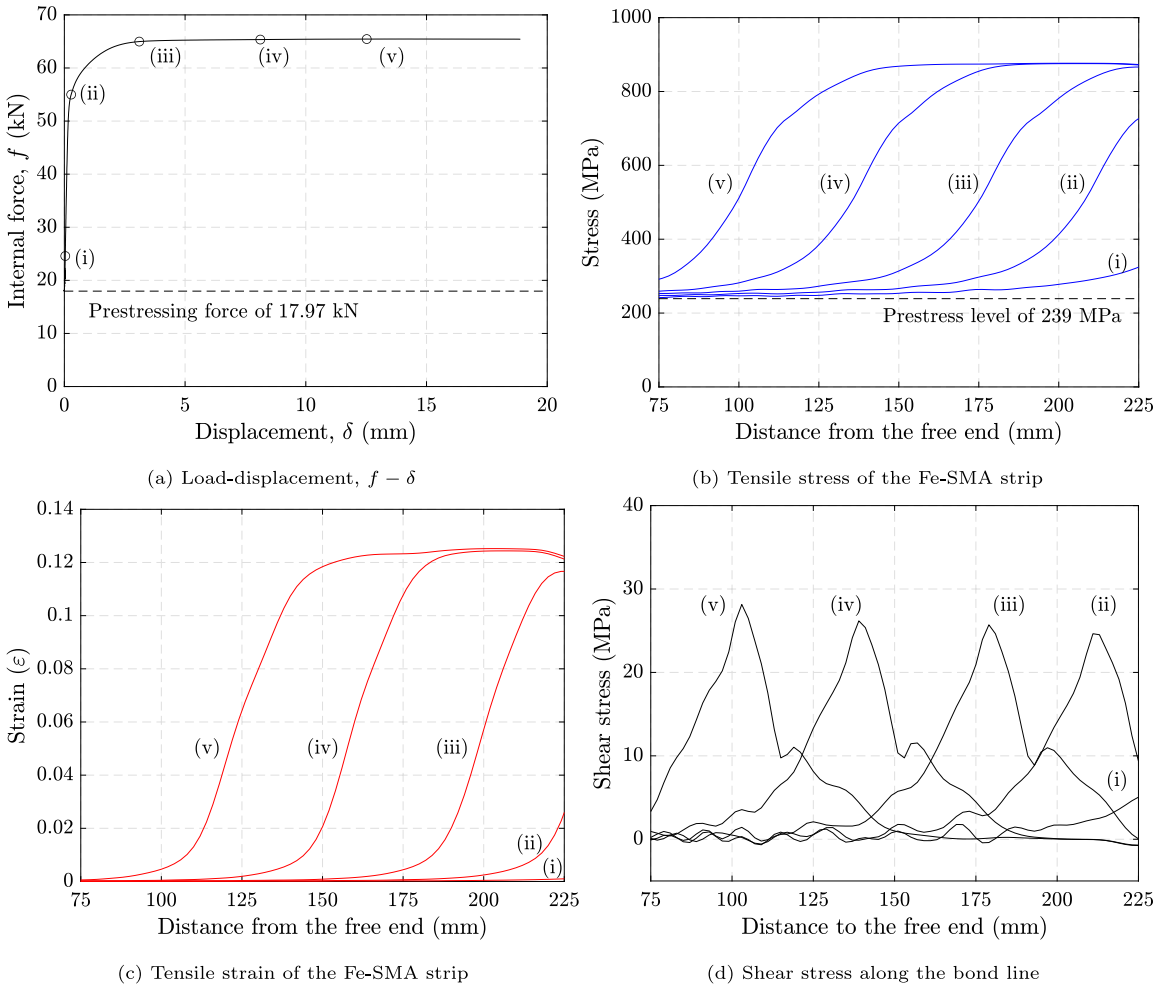

(a) Load-displacement, $f - \delta$

(b) Tensile stress of the Fe-SMA strip

(c) Tensile strain of the Fe-SMA strip

(d) Shear stress along the bond line

Fig. 17. The full-range behavior of PS-ACT180-1, with a prestrained Fe-SMA strip and an activation temperature of 180 °C, neglecting the bonded anchorage zone. Please refer to Fig. 3 for the definition of $f - \delta$. (For interpretation of the references to color in this figure legend, the reader is referred to the web version of this article.)

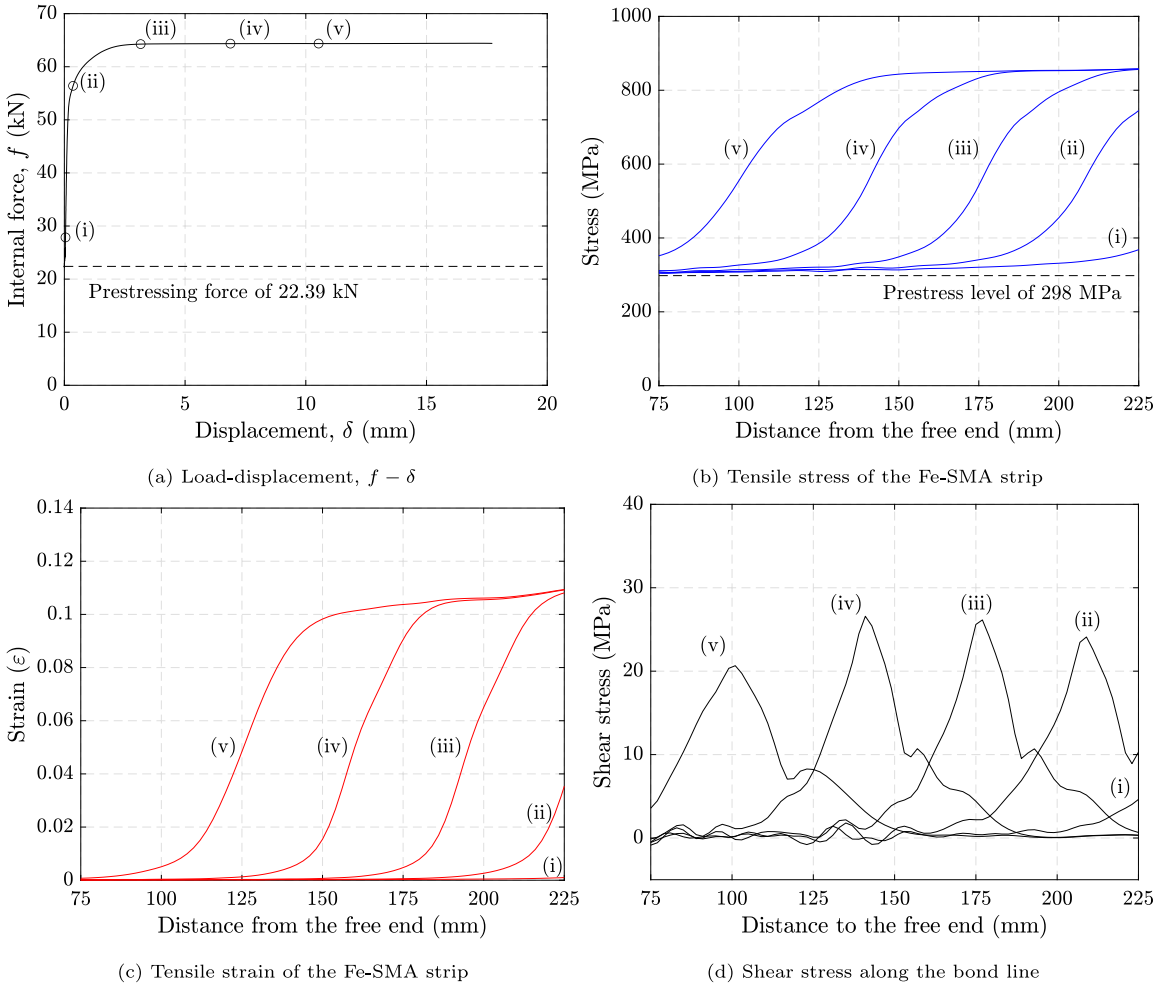

Fig. 18. The full-range behavior of PS-ACT260-1, with a prestrained Fe-SMA strip and an activation temperature of 260 °C, neglecting the bonded anchorage zone. Please refer to Fig. 3 for the definition of $f-\delta$. (For interpretation of the references to color in this figure legend, the reader is referred to the web version of this article.)

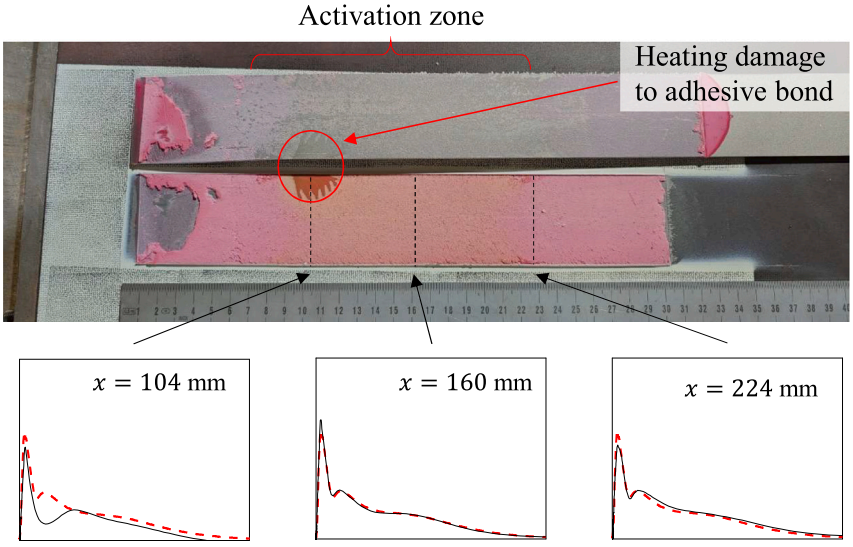

Fig. 19. The fracture surface of specimen PS-ACT260-1 and the measured bond–slip behavior. The dashed red curves are the average bond–slip behavior of the activation zone, while the solid black curves are the local bond–slip behaviors. (For interpretation of the references to color in this figure legend, the reader is referred to the web version of this article.)

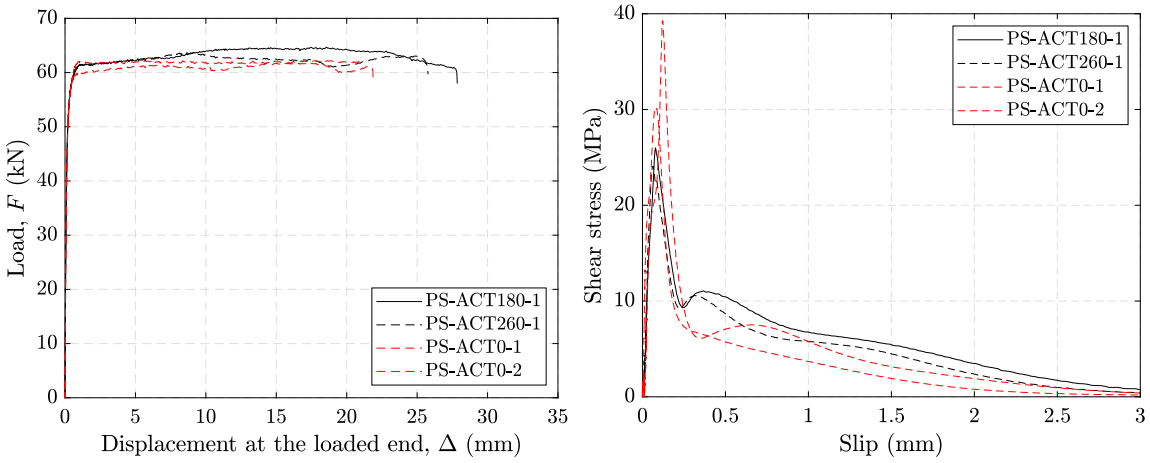

(a) Load-displacement, $F - \Delta$ (b) Bond-slip behavior

Fig. 20. Comparison among joints with (black) and without (red) activation. Tensile forces were measured by a load cell. Please refer to Fig. 3 for the definition of $F - \Delta$. (For interpretation of the references to color in this figure legend, the reader is referred to the web version of this article.)

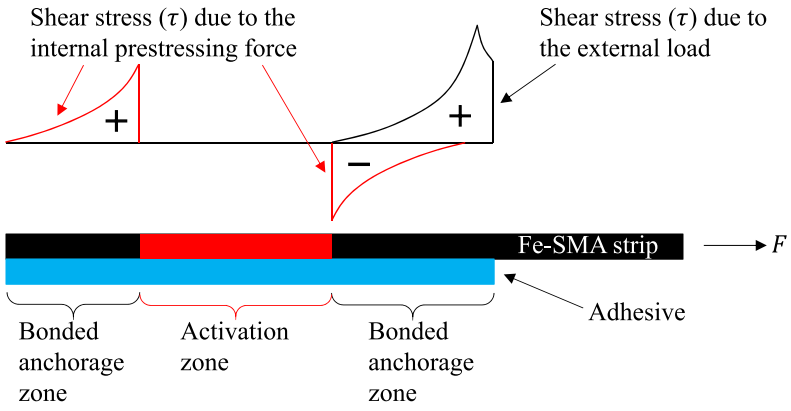

Fig. 21. Schematic view of shear stress distribution due to the prestressing effect and external load (the substrate steel plate not shown). The sign of shear stress refers to the direction: positive implies an orientation towards the right, correspondingly negative implies an orientation towards the left. (For interpretation of the references to color in this figure legend, the reader is referred to the web version of this article.)

4.5.3. Comparison with non-activated specimens

Fig. 20 provides a comparison among the specimens comprising prestrained Fe-SMA strips, with and without the partial activation. Regardless of some noted deviations, the global load–displacement behaviors and local bond–slip curves of these joints are similar, across different joints. This suggests that, despite the generated prestress and temperature effect, the behavior of bonded joints without activation can be adopted in joints with partial activation.

Fig. 21 shows a schematic view of the shear stress distributions in a specimen with partial activation across the entire bond length. The generated prestress over the activation zone attracts Fe-SMAs at the two bonded anchorage zones. As a result, the adhesive in the bonded anchorage zone at the loaded side is sheared towards the left (negative). Under the external tensile load, the adhesive in this bonded anchorage zone is sheared towards the right (positive). To debond this anchorage zone, the adhesive layer needs to be sheared from the negative to the positive direction and eventually up to failure, indicating more effort. However, due to the presence of nonlinearity in both the adherent and the adhesive, the eventual bond capacity does not form a mere superposition of (i) the bond capacity without activation and (ii) the internal prestressing force. Fig. 20(a) shows that the increase of the bond capacity due to the internal prestressing load is negligible. If the bonded anchorage zone becomes lengthier, these two shear stress profiles with different signs do not even superpose on each other, as was demonstrated by Wang et al. [21] via a numerical simulation.

4.6. Further discussions

The effects of the activation temperature and generated prestress on the Fe-SMA-to-steel bonded joints are summarized in Fig. 22. The fracture energy, which is the energy needed to create new unit surface (i.e., debonding or crack), is computed as the area covered under the bond–slip curve. As can be seen in Fig. 22(a), in both groups with non-prestrained (blue) and prestrained (red) Fe-SMAs, an activation to 180 °C enhances the fracture energy. This is similar to the post-curing effect, with which the adhesive, after exposure to an elevated temperature for a certain period of time, improves in terms of its deformation capacity and fracture energy [43–46]. However, when the activation temperature rises at 260 °C, a reduction in fracture energy occurs. Given that the adhesive in the activation zone, at a temperature of 260 °C, changes in color from originally pink to a noticeable yellow, while such a phenomenon is mild for an activation temperature of 180 °C, it can be speculated that the adhesive properties are heavily influenced by the activation temperature. Sika AG [32] reported on a similar phenomenon in the lap-shear strength of bonded joints after exposure to an elevated temperature for one hour; after an exposure to 180 °C, 200 °C, and 220 °C, a zero, 5%, and 25% reduction of the lap-shear strength was found, respectively. These phenomena suggest 180 °C as a proper choice of the activation temperature for this SikaPower 1277 adhesive, so that no damage occurs to the adhesive bond. Comparing the red (with prestress) and blue (without prestress)

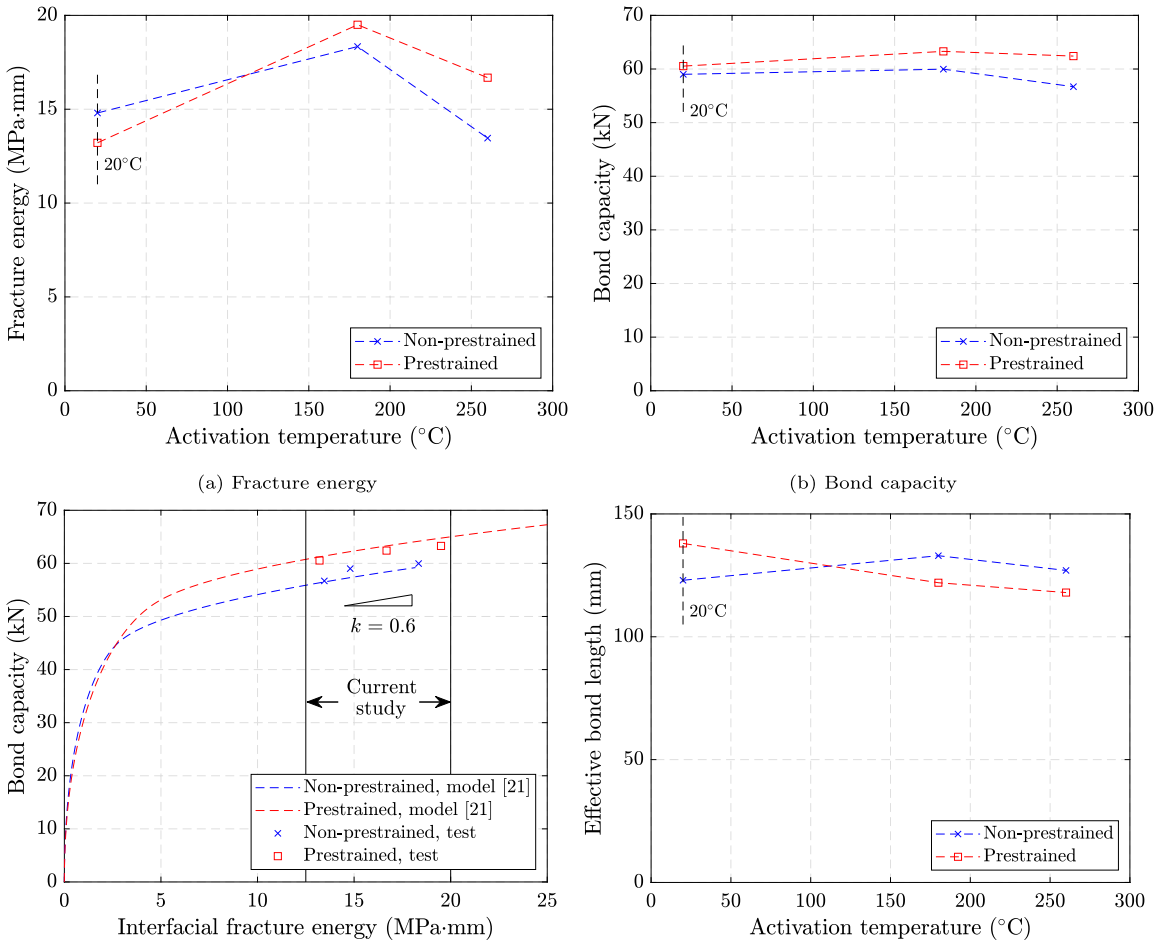

(a) Fracture energy

(b) Bond capacity

(c) Bond capacity as a function of fracture energy, model adopted from Li et al. [25]

(d) Effective bond length

Fig. 22. The effect of activation on the fracture energy, bond capacity, and effective bond length. The vertical dashed line at 20 °C means the room temperature, at which no activation effect is introduced. (For interpretation of the references to color in this figure legend, the reader is referred to the web version of this article.)

curves, it seems that the existence of prestress further enhances the fracture energy. Since the mechanism is not yet clear, the authors tend to ignore its positive effect at the moment and consider this as a safety margin.

Fig. 22(b) manifests that, despite the known change of the fracture energy, the activation has a negligible effect on the bond capacity. In a previous study [25], it was found that the bond capacity of Fe-SMA-to-steel joints is less sensitive to gradients in fracture energy at high values, as compared with the behavior at low fracture energies; this is illustrated in Fig. 22(c). When the fracture energy is larger than 5 MPa· mm, the changing rate of bond capacity is ca. 0.6 kN/(MPa· mm), while that at low fracture energies (lower than 2.5 MPa· mm) is ca. 11 kN/(MPa· mm). As a result, there is no clear change in the bond capacity prior to and after an activation. This further suggests the possibility of employing the bond behavior of a non-activated joint in the design of the bonded Fe-SMA strengthening with activation (within a certain range of activation temperature).

The effect of the activation on the effective bond length is demonstrated in Fig. 22(d). The effective bond length, over which the tensile load is transferred via shear stress to the substrate, does not change with a clear trend with the activation temperature.

5. Conclusion

In this study, six Fe-SMA-to-steel bonded joints were heated via electrical heating, to simulate the activation process of generating prestress. Four joints with bonded anchorage zones survived, while the further two, without bonded anchorage zones, failed due to thermal stresses. Lap-shear tests were then conducted on the surviving four, to characterize the bond behavior between Fe-SMA strips and steel substrates, with the effects of the activation temperature and generated prestress. The following conclusions can be drawn:

1. In bonded Fe-SMA strengthening with local activation, the prevention of a debonding failure during the activation necessitates bonded anchorage zones.
2. The global load–displacement and local bond–slip behavior of the joints prior to and after activation are nearly identical. It applies to joints with non-prestrained and prestrained Fe-SMA strips. This reveals the potential in employing the bond–slip behavior of non-activated joints in the design of bonded Fe-SMA strengthening, where the prestress is generated via heating and cooling.
3. In joints comprising non-prestrained Fe-SMA strips, an activation does not significantly affect the full-range behavior, apart from the local heating damage. However, in joints with prestrained Fe-SMA strips, activation raises the base tensile stress to the level of prestress, while the remaining full-range behavior remains similar to those without activation.
4. The activation temperature introduces some adhesion failure in the activation zone. Although it does not influence the bond behavior in the short-term, its long-term influence (such as

the corrosion resistance) shall be considered in future studies. At locations which lie in direct contact with electrical copper clamps, local heating damages are likely to be induced in the form of local debonding prior to lap-shear tests.

5. The fracture energy of the adhesive bond first increases and then decreases with the activation temperature, while the increased fracture energy is believed to be attributed to a post-curing effect. The bond capacity and effective bond length are barely affected by the activation.
6. 180 °C is regarded as a proper activation temperature for SikaPower 1277 adhesive, as no clear damage is introduced to the adhesive bond.

CRediT authorship contribution statement

Lingzhen Li: Writing – original draft, Methodology, Investigation, Formal analysis, Conceptualization. **Eleni Chatzi:** Writing – review & editing, Supervision, Formal analysis, Conceptualization. **Christoph Czaderski:** Writing – review & editing, Formal analysis. **Elyas Ghafoori:** Writing – review & editing, Supervision, Formal analysis, Conceptualization.

Declaration of competing interest

The authors declare that they have no known competing financial interests or personal relationships that could have appeared to influence the work reported in this paper.

Data availability

Data will be made available on request.

Acknowledgments

The authors acknowledge the China Scholarship Council (CSC) for co-financing the PhD project of the first author. re-fer AG and Sika AG are appreciated to provide Fe-SMA and adhesive materials, respectively. Special thanks go to Mr. André Kupferschmid from the Transport at Nanoscale Interfaces Laboratory at Empa and Mr. Giovanni Saragoni and Mr. Robert Widmann in the Bauhalle team at Empa for their technical support.

Appendix. Simplified thermal analysis

A.1. Model setup

This section provides an analytical solution of the thermal stress in the bond line, quantitatively explaining the debonding phenomenon in group (i), where the Fe-SMA strips are non-prestrained, and no prestressing effect is expected. During the electrical resistance heating, the temperature in the Fe-SMA strips raised to 180 °C or 260 °C, while that in steel plates remained low. This is different from many of the existing thermal analyses of adhesively bonded joints [47–49], where adherent strips (such as CFRP strips) and substrates (such as concrete cylinders and steel plates) were heated simultaneously. Given the fact that (i) the steel substrate is much (ca. 43 times) stiffer than the Fe-SMA strip and (ii) the temperature in the steel substrate has negligible change during the ascending temperature of the Fe-SMA strip, the steel plate is regarded as a fixed foundation, and the analysis is simplified as a joint illustrated in Fig. A.23.

The equilibrium of an Fe-SMA element reads Eq. (A.1). If the adhesive layer is infinite rigid, where the Fe-SMA strip is not allowed for any thermal expansion, the stress in the Fe-SMA strip reads $\sigma^* = -E{\cdot}\alpha{\cdot}\Delta T$ (a compressive state). In reality, the adhesive has a finite stiffness, which reduces at an elevated temperature. Therefore, the adhesive layer

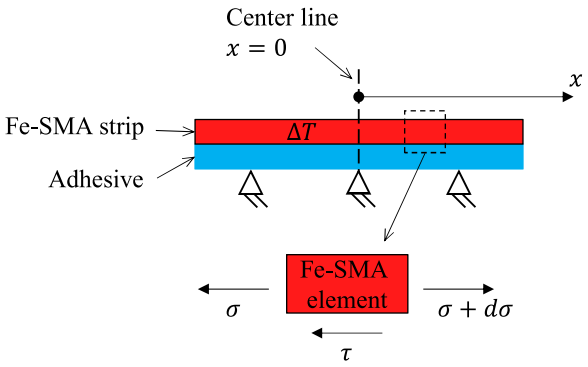

Fig. A.23. Simplification of a bonded Fe-SMA joint in the ascending temperature and the equilibrium state of an Fe-SMA element. The Fe-SMA strip is heated along the entire bond length, while the steel substrate is regarded as a fixed foundation without temperature change. (For interpretation of the references to color in this figure legend, the reader is referred to the web version of this article.)

deforms in shear, while the compression in the Fe-SMA strip releases, and the stress in the Fe-SMA strip can be expressed as Eq. (A.2). Since the adhesive properties at high temperatures, i.e., 180 °C and 260 °C, are unknown, an ascending bond–slip behavior is assumed, as written per Eq. (A.3).

$$\frac{\mathrm{d}\sigma}{\mathrm{d}x} = \frac{\tau}{t} \tag{A.1}$$

$$\sigma = E \cdot \frac{\mathrm{d}s}{\mathrm{d}x} - E \cdot \alpha \cdot \Delta T \tag{A.2}$$

$$\tau = k \cdot s \tag{A.3}$$

where σ and τ represent the tensile and shear stresses, respectively; t and x denote the thickness of the Fe-SMA strip and the coordinate in the longitudinal direction, respectively; E denotes the E-modulus of the Fe-SMA in the quasi-linear stage; s and k represent the slip and shear stiffness, respectively; α and ΔT are the thermal expansion coefficient and the amount of elevated temperature, respectively.

Substituting Eqs. (A.2) and (A.3) into Eq. (A.1) yields

$$\frac{\mathrm{d}^2 s}{\mathrm{d}x^2} - \omega^2 \cdot s = 0 \tag{A.4}$$

where $\omega = \sqrt{\frac{k}{E \cdot t}}$.

Two boundary conditions are defined as follows. (i) Due to the symmetry, the slip at the center of the bond ($x = 0$) is zero, noted as Eq. (A.5). (ii) At the free end ($x = L$), the tensile stress of the Fe-SMA is zero, expressed as Eq. (A.6).

$$s|_{x=0} = 0 \tag{A.5}$$

$$\sigma|_{x=L} = 0 \tag{A.6}$$

A solution, which reads Eq. (A.7), is assumed for slip.

$$s = A \cdot \exp(B \cdot x) + C \cdot \exp(D \cdot x) \tag{A.7}$$

Substituting the two boundary conditions (Eqs. (A.5) and (A.6)) into Eqs. (A.2) and (A.7), respectively, leads to the solution of slip, which reads Eq. (A.8), with a reformulation of Eq. (A.9).

$$s = \frac{\alpha \cdot \Delta T}{\omega} \cdot \frac{\exp(\omega \cdot x) - \exp(-\omega \cdot x)}{\exp(\omega \cdot L) + \exp(-\omega \cdot L)} \tag{A.8}$$

$$s = \frac{\alpha \cdot \Delta T}{\omega} \cdot \frac{\sinh(\omega \cdot x)}{\cosh(\omega \cdot L)} \tag{A.9}$$

Accordingly, the solution of tensile strain and stress read Eqs. (A.10) and (A.11), respectively.

$$\varepsilon = \alpha \cdot \Delta T \cdot \frac{\cosh(\omega \cdot x)}{\cosh(\omega \cdot L)} \tag{A.10}$$

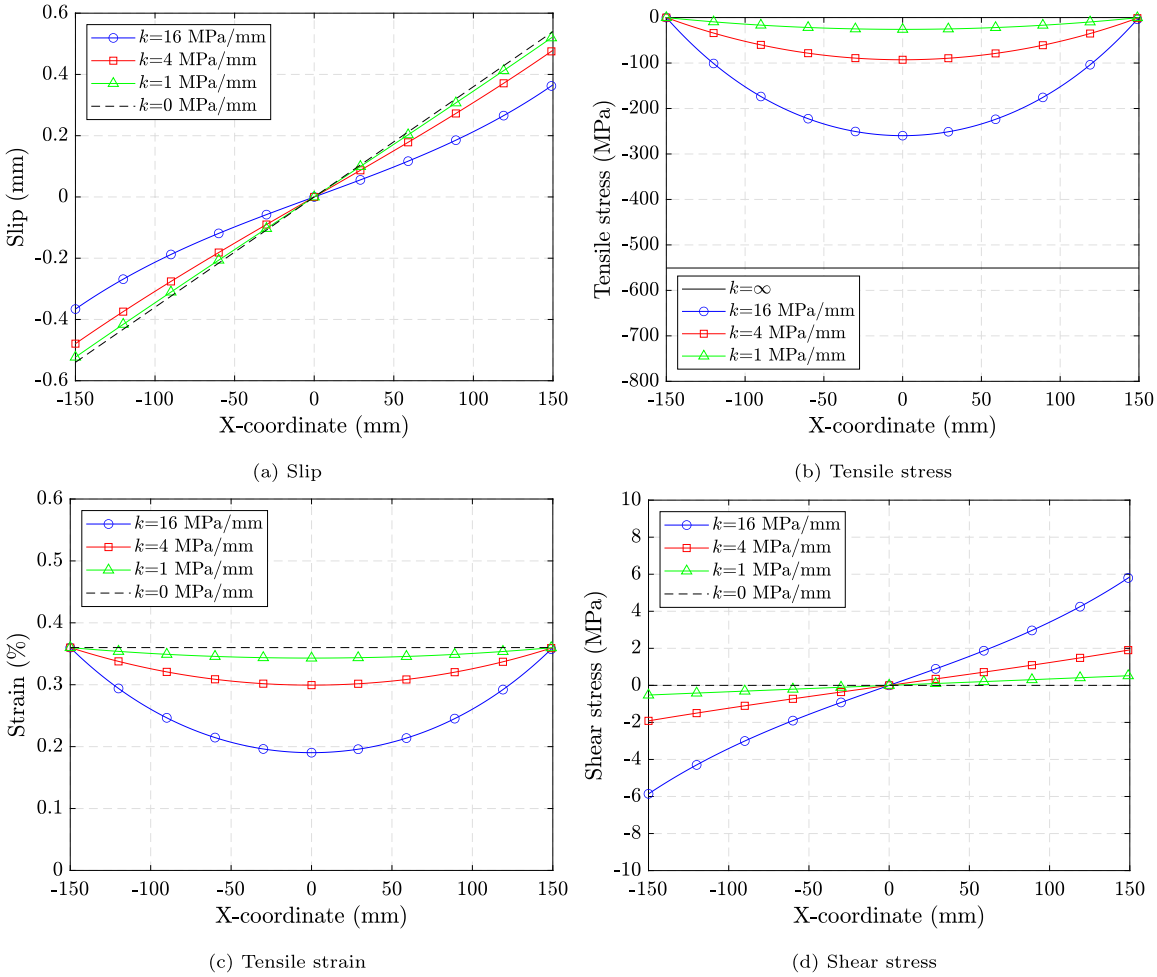

Fig. A.24. Behavior at the target activation temperature, with T_{act} = 260 °C as an example. Please refer to Fig. A.23 for the x−coordinate. Sign of slip and shear stress refer to the direction. The slip is positive to the right and negative to the left, while the shear stress is positive to the left and negative to the right. (For interpretation of the references to color in this figure legend, the reader is referred to the web version of this article.)

$$\sigma = E \cdot \alpha \cdot \Delta T \cdot \left[\frac{\cosh(\omega \cdot x)}{\cosh(\omega \cdot L)} - 1\right] \tag{A.11}$$

A.2. Analysis

specimens. An E-modulus of 153 GPa, representing the quasi-linear stage of the non-prestrained Fe-SMA [24], and a thermal expansion coefficient of 1.5×10^{-5}/°C [50,51] are adopted in the analysis. Fig. A.24 illustrates the thermal deformation and stresses at the target activation temperature of NS-ACT260-1, as an example in group (i).

In the thermal analysis, a key parameter is the shear stiffness in the adhesive layer. Three virtual joints are assumed here, with reduced shear stiffness to different degrees. According to Sika technical data sheets [31,32], the storage modulus and shear strength have a reduction of 96% and 83%, respectively, at 120 °C, see Fig. 5. Given a shear stiffness of 400 MPa/mm and a lap-shear strength of 20 MPa at the room temperature [25], the first virtual joint corresponding to the adhesive properties at 120 °C is assumed to possess a shear stiffness and shear strength of 16 MPa/mm and 3.4 MPa, respectively. The result of the first virtual joint is illustrated as blue curve with circular marks in Fig. A.24. The thermal stress is released by ca. 50% at the center of the bond line (x = 0), compared against a joint with a rigid bond (k = ∞). At the center of the bond line, the thermal expansion strain is approximately half of the case with a free bond (k = 0). The shear stress at the two ends are 5.9 MPa, which exceeds the lap-shear strength of 3.4 MPa at 120 °C. This means that an activation to 260 °C and assuming the material properties at 120 °C lead to severe damage at the two ends of the bond line.

The shear stiffness and lap-shear strength, which should further reduce in reality, are unavailable. Therefore, the second and third virtual joints are assumed with a shear stiffness of 4 MPa/mm and 1 MPa/mm, respectively, corresponding to a reduction of 99% and 99.75%, respectively. The behavior of these two virtual joints are illustrated as red curves with square marks and green curves with triangular marks, respectively, in Fig. A.24. In these two joints, the thermal expansion of the Fe-SMA is further released, while the compressive stress in the Fe-SMA strip and the shear stress along the bond line remain low. He et al. [39] collected 106 CFRP bonded lap-shear joints at different temperatures, ranging from 20 to 120 °C, and summarized a model (Eqs. (A.12) and (A.13)) for the prediction of bond capacity at elevated temperatures.

$$F_b(T) = \gamma \cdot F_{b,r} \tag{A.12}$$

$$\gamma = \frac{f_1}{1 + \exp[(T - T_g - T_r)/f_2]} \tag{A.13}$$

where T_r and T denote the room temperature, which equals 23 °C, and an elevated temperature, respectively; $F_{b,r}$ and $F_b(T)$ refer to the bond capacities at the room temperature and elevated temperature, respectively; γ denotes the ratio of the bond capacity at an elevated temperature over that at the room temperature; T_g refers to the glass transition temperature of the adhesive; f_1 and f_2, which equal 0.9 and 8.5, respectively, are two constants from regression.

Though the activation temperatures in the current study exceed the temperature range for regression of Eqs. (A.12) and (A.13), and our adherents are Fe-SMA rather than CFRP, an extrapolation provides an indication of the magnitude of the bond capacity at the target temperatures. The model predicts γ values of 2.3×10^{-5} 1.8×10^{-9} at 180 and 260 °C, respectively, which suggest a zero bond capacity. This means that the zero load transferring capacity at the activation temperature cannot resist any shear stress. As a result, the shear stress illustrated as a red curve with square marks and a green curve with triangular marks in Fig. A.24(d) leads to debonding failure.

References

[1] T. Hong, C. Ji, M. Jang, H. Park, Assessment model for energy consumption and greenhouse gas emissions during building construction, J. Manage. Eng. 30 (2) (2014) 226–235.
[2] Iron and Steel Technology Roadmap: Towards more Sustainable Steelmaking, International Energy Agency, 2020.
[3] H. Nordin, B. Täljsten, Concrete beams strengthened with prestressed near surface mounted CFRP, J. Compos. Constr. 10 (1) (2006) 60–68.
[4] H.Y. Lee, W.T. Jung, W. Chung, Flexural strengthening of reinforced concrete beams with pre-stressed near surface mounted CFRP systems, Compos. Struct. 163 (2017) 1–12.
[5] J. Yang, R. Haghani, M. Al-Emrani, Innovative prestressing method for externally bonded CFRP laminates without mechanical anchorage, Eng. Struct. 197 (2019) 109416.
[6] A. Hosseini, E. Ghafoori, M. Motavalli, A. Nussbaumer, X.-L. Zhao, Mode I fatigue crack arrest in tensile steel members using prestressed CFRP plates, Compos. Struct. 178 (2017) 119–134.
[7] Y. Huawen, C. König, T. Ummenhofer, Q. Shizhong, R. Plum, Fatigue performance of tension steel plates strengthened with prestressed CFRP laminates, J. Compos. Constr. 14 (5) (2010) 609–615.
[8] T. Chen, X.-L. Gu, M. Qi, Q.-Q. Yu, Experimental study on fatigue behavior of cracked rectangular hollow-section steel beams repaired with prestressed CFRP plates, J. Compos. Constr. 22 (5) (2018) 04018034.
[9] L. Hu, P. Feng, Prestressed CFRP-reinforced steel columns under axial and eccentric compression, Compos. Struct. 268 (2021) 113940.
[10] L. Janke, C. Czaderski, M. Motavalli, J. Ruth, Applications of shape memory alloys in civil engineering structures—Overview, limits and new ideas, Mater. Struct. 38 (2005) 578–592.
[11] A. Cladera, B. Weber, C. Leinenbach, C. Czaderski, M. Shahverdi, M. Motavalli, Iron-based shape memory alloys for civil engineering structures: An overview, Constr. Build. Mater. 63 (2014) 281–293.
[12] W.J. Lee, B. Weber, G. Feltrin, C. Czaderski, M. Motavalli, C. Leinenbach, Stress recovery behaviour of an Fe–Mn–Si–Cr–Ni–VC shape memory alloy used for prestressing, Smart Mater. Struct. 22 (12) (2013) 125037.
[13] B. Schranz, J. Michels, C. Czaderski, M. Motavalli, T. Vogel, M. Shahverdi, Strengthening and prestressing of bridge decks with ribbed iron-based shape memory alloy bars, Eng. Struct. 241 (2021) 112467.
[14] A. Cladera, L.A. Montoya-Coronado, J.G. Ruiz-Pinilla, C. Ribas, Shear strengthening of slender reinforced concrete T-shaped beams using iron-based shape memory alloy strips, Eng. Struct. 221 (2020) 111018.
[15] M.R. Izadi, E. Ghafoori, M. Motavalli, S. Maalek, Iron-based shape memory alloy for the fatigue strengthening of cracked steel plates: Effects of re-activations and loading frequencies, Eng. Struct. 176 (2018) 953–967.
[16] W. Wang, L. Li, A. Hosseini, E. Ghafoori, Novel fatigue strengthening solution for metallic structures using adhesively bonded Fe–SMA strips: A proof of concept study, Int. J. Fatigue 148 (2021) 106237.
[17] L. Li, S. Wang, T. Chen, E. Chatzi, H. Heydarinouri, E. Ghafoori, Fatigue strengthening of cracked steel plates with bonded Fe–SMA strips, ce/papers 6 (3–4) (2023) 380–384.
[18] B. Zheng, M. Dawood, Fatigue strengthening of metallic structures with a thermally activated shape memory alloy fiber-reinforced polymer patch, J. Compos. Constr. 21 (4) (2017) 04016113.
[19] L. Li, T. Chen, X. Gu, E. Ghafoori, Heat activated SMA-CFRP composites for fatigue strengthening of cracked steel plates, J. Compos. Constr. 24 (6) (2020) 04020060.
[20] J. Deng, Z. Fei, J. Li, H. Li, Fatigue behaviour of notched steel beams strengthened by a self-prestressing SMA/CFRP composite, Eng. Struct. 274 (2023) 115077.
[21] S. Wang, L. Li, Q. Su, X. Jiang, E. Ghafoori, Strengthening of steel beams with adhesively bonded memory-steel strips, Thin-Walled Struct. 189 (2023) 110901.
[22] J. Vůjtěch, P. Ryjáček, J.C. Matos, E. Ghafoori, Iron-based shape memory alloy for strengthening of 113-year bridge, Eng. Struct. 248 (2021) 113231.
[23] W. Wang, A. Hosseini, E. Ghafoori, Experimental study on Fe–SMA-to-steel adhesively bonded interfaces using DIC, Eng. Fract. Mech. 244 (2021) 107553.
[24] L. Li, W. Wang, E. Chatzi, E. Ghafoori, Experimental investigation on debonding behavior of Fe–SMA-to-steel joints, Constr. Build. Mater. 364 (2023) 129857.
[25] L. Li, E. Chatzi, E. Ghafoori, Debonding model for nonlinear Fe–SMA strips bonded with nonlinear adhesives, Eng. Fract. Mech. 282 (2023) 109201.
[26] Z. Dong, U.E. Klotz, C. Leinenbach, A. Bergamini, C. Czaderski, M. Motavalli, A novel Fe–Mn–Si shape memory alloy with improved shape recovery properties by VC precipitation, Adv. Eng. Mater. 11 (1–2) (2009) 40–44.
[27] L. Li, S. Wang, E. Chatzi, M. Motavalli, E. Ghafoori, Prediction of prestress level in steel structures strengthened by bonded Fe–SMA strips, ce/papers 6 (3–4) (2023) 364–368.
[28] E. Ghafoori, E. Hosseini, C. Leinenbach, J. Michels, M. Motavalli, Fatigue behavior of a Fe–Mn–Si shape memory alloy used for prestressed strengthening, Mater. Des. 133 (2017) 349–362.
[29] B. Schranz, C. Czaderski, M. Shahverdi, J. Michels, T. Vogel, M. Motavalli, Ribbed iron-based shape memory alloy bars for pre-stressed strengthening applications, in: International Association for Bridge and Structural Engineering Symposium, Guimaraes, Portugal, 2019.
[30] L. Zerbe, D. Vieira, A. Belarbi, A. Senouci, Uniaxial compressive behavior of circular concrete columns actively confined with Fe–SMA strips, Eng. Struct. 255 (2022) 113878.
[31] A.G. Sika, Additional product information, SikaPower-1277, version 1, 2018.
[32] A.G. Sika, Additional product information, SikaPower-1277, version 2, 2018.
[33] A. Franck, T.I. Germany, Viscoelasticity and dynamic mechanical testing, 1993, TA Instruments, New Castle, de, USA AN004.
[34] ISO 4587:2003, Adhesives — Determination of tensile lap-shear strength of rigid-to-rigid bonded assemblies, 2003.
[35] B. Schranz, C. Czaderski, T. Vogel, M. Shahverdi, Bond investigations of pre-stressed, near-surface-mounted, ribbed memory-steel bars with full bond length, Mater. Des. 196 (2020) 109145.
[36] L. Li, Bond behavior and debonding failure in Fe–SMA strengthened steel members, ETH Zurich, 2023.
[37] N. Pichler, W. Wang, J.A. Poulis, E. Ghafoori, Surface preparations and durability of iron-based shape memory alloy adhesively-bonded joints, Int. J. Adhes. Adhes. 125 (2023) 103439.
[38] M. Leone, S. Matthys, M.A. Aiello, Effect of elevated service temperature on bond between FRP EBR systems and concrete, Composites B 40 (1) (2009) 85–93.
[39] J. He, G. Xian, Y.X. Zhang, Effect of moderately elevated temperatures on bond behaviour of CFRP-to-steel bonded joints using different adhesives, Constr. Build. Mater. 241 (2020) 118057.
[40] M. Shahverdi, J. Michels, C. Czaderski, M. Motavalli, Iron-based shape memory alloy strips for strengthening RC members: Material behavior and characterization, Constr. Build. Mater. 173 (2018) 586–599.
[41] X.-L. Gu, Z.-Y. Chen, Q.-Q. Yu, E. Ghafoori, Stress recovery behavior of an Fe–Mn–Si shape memory alloy, Eng. Struct. 243 (2021) 112710.
[42] M.R. Izadi, E. Ghafoori, M. Shahverdi, M. Motavalli, S. Maalek, Development of an iron-based shape memory alloy (Fe–SMA) strengthening system for steel plates, Eng. Struct. 174 (2018) 433–446.
[43] S. Mostovoy, E.J. Ripling, Fracture toughness of an epoxy system, J. Appl. Polym. Sci. 10 (9) (1966) 1351–1371.
[44] S. Mostovoy, E.J. Ripling, C.F. Bersch, Fracture toughness of adhesive joints, J. Adhes. 3 (2) (1971) 125–144.
[45] R.J.C. Carbas, L.F.M. Da Silva, E.A.S. Marques, A.M. Lopes, Effect of post-cure on the glass transition temperature and mechanical properties of epoxy adhesives, J. Adhes. Sci. Technol. 27 (23) (2013) 2542–2557.
[46] X. Han, Y. Chao, W. Zhang, Y. Chao, C. Wu, Study on the effect of post curing on the mode II fracture energy of structural adhesive using a parameter identification approach, Int. J. Adhes. Adhes. 95 (2019) 102398.
[47] W.Y. Gao, J.G. Teng, J.-G. Dai, Effect of temperature variation on the full-range behavior of FRP-to-concrete bonded joints, J. Compos. Constr. 16 (6) (2012) 671–683.
[48] H. Zhou, J.P. Torres, D. Fernando, A. Law, R. Emberley, The bond behaviour of CFRP-to-steel bonded joints with varying bond properties at elevated temperatures, Eng. Struct. 183 (2019) 1121–1133.
[49] H.C. Biscaia, C. Chastre, A. Viegas, N. Franco, Numerical modelling of the effects of elevated service temperatures on the debonding process of FRP-to-concrete bonded joints, Composites B 70 (2015) 64–79.
[50] E. Hosseini, E. Ghafoori, C. Leinenbach, M. Motavalli, S.R. Holdsworth, Stress recovery and cyclic behaviour of an Fe–Mn–Si shape memory alloy after multiple thermal activation, Smart Mater. Struct. 27 (2) (2018) 025009.
[51] K. Hong, S. Lee, S. Han, Y. Yeon, Evaluation of Fe-based shape memory alloy (Fe–SMA) as strengthening material for reinforced concrete structures, Appl. Sci. 8 (5) (2018) 730.